MSc Thesis Civil Engineering and Management
River & Coastal Engineering

# Assessment of the influence of incident wind angle and dune slope inclination on sediment transport patterns in coastal dunes

Abraham J. Jonkheer

Head graduation committee:
Prof. Dr. S.J.M.H. Hulscher

Supervisors:
Dr. ir. M.W.J. Smit (Witteveen+Bos)
ir. P. Pourteimouri
Dr. ir. G.H.P. Campmans

August, 2022

UNIVERSITY OF TWENTE.

Witteveen + Bos

Department of Civil Engineering and Management
Faculty of Engineering Technology

# Preface

This MSc thesis is part of my graduation project for the MSc Civil Engineering and Management at the University of Twente, with the focus on River & Coastal Engineering. The research project was conducted in collaboration with the company Witteveen+Bos, under supervision of Marije Smit. At the University of Twente, the project was supervised by Paran Pourteimouri, Geert Campmans and Suzanne Hulscher.

I would like to thank everyone who has helped me during the time I worked on this MSc thesis.

First of all, I want to thank God for His help and support. You helped me in the times when I felt down and You gave me a reason to keep going on the right track. I want to thank Roos, my wife, for supporting and loving me through all the months I have put into this research. I was not always the best husband when my mind was fully occupied by this research, but you were always there.

I also want to thank all the colleagues I have had the chance to get to know at Witteveen+Bos. For the times during lunch to just chat about all kinds of things, but also for the help I received by discussing my research. In particular, I want to thank Marije for her help on this research. Although we did not see each other often in real life, the online meetings have helped me stay focused and on track throughout the project.

Thank you, Paran and Geert, for supervising me throughout this research and helping me where I got stuck. The weekly meetings were very helpful to me to keep going on the right track. Thank you, Suzanne, for being willing to fill in as committee chair and helping me steer towards a better quality research.

Moreover, I want to thank my parents for always being supportive and encouraging me to get the best out of myself. Also, I want to thank my parents-in-law for the weekends in Lelystad, where I could relax and always feel at home.

Thank you, Casper, Chris, Tim and Benny, for a great vacation to help me relax before the final stretch of my graduation project.

Finally, I want to thank all the people with whom I worked on my thesis at the university. Andries, Vanja, Cathy and Jedidja, thank you for just being there to work together and sometimes give a nice distraction from the work by going for a walk.

I hope you will find this report interesting and educational, and of course that you will enjoy yourself while reading it.

Sincerely, Bram Jonkheer

*Enschede, August 2022*

# Summary

For the protection of coasts, hard structures such as dikes and groynes have been important tools over the past centuries. In more recent years, the use of natural and 'soft' solutions has increased as measures to improve coastal safety, which is generally referred to as Building with Nature. A nice example can be found at the Dutch coast. When it was established that the coastal defense system had a weak link between Petten and Camperduin, a sandy solution was chosen for this location, instead of reinforcing the existing hard construction. For the development of this system, called the Hondsbossche Dunes, estimations were made to predict the evolution of the dunes and the beach. However, the impact of dune slope inclination, longshore variability in the shape of the dunes and the influence of the dominant wind direction at the beach relative to the dunes, were not fully known and therefore estimations were made based on the available knowledge.

In this thesis, research into the influence of incident wind angle and slope inclination on wind flow patterns and sediment transport patterns on dunes and steep slopes is presented. The research is done using a 3D CFD (Computational Fluid Dynamics) model in OpenFOAM. The incident wind angle (relative to the dune toe) is varied between 0° (normal to the dune toe) and 75°, with steps of 15°. The dune slope inclination is varied from 10° to 80°, with steps of 10°. A systematic procedure is used to create smooth transitions over the beach-dune profile, at the dune toe and dune crest. This is different from previous CFD studies, in which sharp edges have been used. Moreover, there has never been research fully dedicated to assessing the combined impact of the slope inclination and incident wind angle on the flow and sediment transport patterns over dunes.

The results show adequate reproduction of air flow dynamics over the dune profile, by comparing the results to previous research. Flow separation at the dune toe and on the dune crest has been shown, giving rise to three different possible flow regimes, depending on the incident wind angle and dune slope inclination. The results found on the sediment transport over the dune profile show a strong dependency on both the incident wind angle and the slope inclination. Moreover, it is shown that the combination of the two parameters can lead to different sediment transport dynamics at different locations on the dune profile.
Sedimentation around the toe of an unvegetated dune is shown to be largest for a slope inclination of 20° and an incident wind angle of 0°. On the other hand, it is shown that, for most incident wind angles, a large amount of erosion on the dune slope can be expected when vegetation is not present. However, the inclusion of vegetation in the model leads to results that are comparable to the field data from the Hondsbossche Dunes project. Finally, advice is given and recommendations for further research are presented on how to use this research for practical predictions of sedimentation and erosion on a dune profile.

In conclusion, this thesis results in a better understanding of both flow dynamics and sediment transport patterns over dunes and steep slopes under different wind directions and for slope inclinations.

*Keywords*: Computational Fluid Dynamics, Building with Nature, Aeolian sediment transport, Air flow patterns, 3D Modeling, Coastal Dunes, OpenFOAM

# Contents

# List of Figures

# List of Tables



# List of symbols

| Symbol | Description | Unit |
|---|---|---|
| $A$ | Constant for slope adjustment equation | - |
| $\alpha$ | Sediment friction angle | $^\circ$ |
| $C$ | Constant for sediment transport equation | - |
| $\gamma$ | Dune slope inclination | $^\circ$ |
| $\gamma_{\text{rel}}$ | Dune slope inclination relative to the flow direction | $^\circ$ |
| $d$ | Mean sediment grain size | m |
| $D$ | Reference grain diameter | m |
| $DW$ | Cross-shore dune width | m |
| $\Delta t$ | Time step for profile update | s |
| $\epsilon$ | Turbulence dissipation rate | $m^2/s^3$ |
| $g$ | Gravitational acceleration on Earth | $m/s^2$ |
| $\theta$ | Incident wind angle at the inlet | $^\circ$ |
| $\theta_w$ | Flow direction (varying over the domain) | $^\circ$ |
| $\theta_\tau$ | Shear stress direction | $^\circ$ |
| $k$ | Turbulent kinetic energy | $m^2/s^2$ |
| $\kappa$ | Von Kármán constant | - |
| $n$ | Sediment porosity | - |
| $q$ | Sediment transport magnitude | kg/m/s or $m^3$/m/month |
| $q_x$ | Sediment transport in cross-shore direction | kg/m/s or $m^3$/m/month |
| $q_y$ | Sediment transport in longshore direction | kg/m/s or $m^3$/m/month |
| $\rho_a$ | Density of air | $kg/m^3$ |
| $\rho_s$ | Density of sediment | $kg/m^3$ |
| $\vec{\tau}$ | Bed shear stress vector in three dimensions ($\tau_x$, $\tau_y$, $\tau_z$) | $N/m^2$ |
| $\vec{U}$ | Flow velocity vector in three dimensions ($U_x$, $U_y$, $U_z$) | m/s |
| $U_{\text{ref}}$ | Reference flow velocity at inlet at 1.8 m above the surface | m/s |
| $u_*$ | Shear velocity | m/s |
| $u_{*,\text{th}}$ | Threshold shear velocity | m/s |
| $x$ | Cross-shore direction coordinate | m |
| $x^*$ | Cross-shore normalized dune slope coordinate ($(x - x_{\text{toe}})/DW$) | - |
| $x_{crest}$ | Cross-shore position of the dune crest | m |
| $x_{toe}$ | Cross-shore position of the dune toe | m |
| $y$ | Longshore direction coordinate | m |
| $z$ | Vertical direction coordinate | m |
| $z_0$ | Surface roughness length | m |
| $z_b$ | Surface level | m |

# 1 Introduction

## 1.1 Context

Coastal areas make up an important part of our globe and are often attractive to people. Many cities have been built close to the coastline, beaches are used for recreational purposes and in many places the nearshore represents an economic asset to the region. On the other hand, coastal areas can be very vulnerable. If there is no flood defense of any kind, a storm can cause a flood, doing damage to communities and even sometimes taking lives. On sandy shores, dunes often play an important role in the natural protection of a coastal area. They act as a natural flood defense to the land behind and create an ecosystem with a variety of plants and wildlife. These natural coastal dune systems provide a defense from the water, but in many places, man-made structures such as groynes and dikes are added to provide more safety. More recently, artificial dunes have also been constructed as a solution for improving coastal safety. For example, a weak part of the Dutch flood defense system, the Pettemer Zeewering, has been strengthened by the placement of 35.6 $Mm^3$ of sand on the foreshore and on the beach, creating a completely new dune system. This was the birth of the Hondsbossche Dunes, giving rise to a new ecosystem along the Dutch coast. The completed project is shown in Figure 1. It can be seen that different dune profiles have been used and that most of the sand has been deployed in front of the old dike (the Pettemer Zeewering). By monitoring the dune profile in the years thereafter, it has shown to be a valuable source for the better understanding of the impact of design choices on sediment transport over an artificial dune system, such as the influence of different dune profiles (Bodde et al., 2019).

Undoubtedly, to design an artificial dune system on the shore in a way that is most sustainable and to be able to predict its development, research is needed to better understand the process that contributes a lot to the morphological evolution of dunes: aeolian sediment transport. There are many parameters that influence the sediment transport patterns over a dune profile. In our study, we explicitly focus on two parameters: the dune slope inclination and the incident wind direction relative to the dunes.

FIGURE 1: The Hondsbossche Dunes flood defense. Adapted from the EcoShape webpage on the Hondsbossche Dunes (https://www.ecoshape.org/nl/pilots/hondsbossche-en-pettemer-zeewering/).

The modeling of flow-driven sediment transport started almost a hundred years ago, and since then researchers have found many empirical relations in the field of sediment transport, many of which are still used today (e.g. Bagnold, 1937; Kawamura, 1951; Lettau and Lettau, 1978). However, a sediment transport equation just offers a potential sediment transport value at a certain location, which can be limited by many factors, such as moisture, vegetation and slope. Moreover, these equations need detailed input to give accurate values, and therefore detailed field experiments are needed to obtain realistic sediment transport values.

However, detailed field experiments are time-consuming and expensive and some parameters are hard to calculate in the field, even with a lot of effort. Numerical simulations can offer a helping hand with these issues. For instance, instead of using estimates of bed shear stresses over the domain by interpolation of a few data points, a shear stress value can be extracted at each point on the domain. Moreover, all parameters can be easily changed and the influence of each can be investigated separately. This shows that, once you know that a numerical model is capable of reproducing reality to a sufficient extent, model simulations are a powerful tool for research into the prediction of something like the sediment transport patterns over a dune. Nowadays, the most common method to perform numerical simulations of near-surface flows is with the use of Computational Fluid Dynamics (Smyth, 2016). However, these models can be computationally expensive, for example when high accuracy is required or when the model domain is large.

There have been studies investigating the influence of wind direction on (shear) velocity and/or sediment transport over slopes (e.g. Davidson et al., 2022; Hesp and Smyth, 2016; Roelvink and Costas, 2019; Smyth and Hesp, 2015). A dune can cause winds to deflect in longshore direction along the dune, or steer towards a more crest-normal direction, depending on the incident wind angle. This will cause a change in both the magnitude and direction of the shear velocity over the entire dune, which in turn influences the sediment transport. Knowledge about these effects can lead to a better design of an artificial dune profile. Furthermore, the impact of the stoss or windward slope inclination on (shear) velocity over slopes has been investigated to some extent (e.g. Hesp and Smyth, 2021; Tsoar et al., 1996). The slope of dunes can create different flow patterns which in turn influence the sedimentation and erosion patterns. However, there has never been research fully dedicated to assessing the combined impact of the dune slope inclination and incident wind angle on the sediment transport in coastal dunes.

## 1.2 Study objective

The context above leads to the following objective of this research: to determine the effect of the incident wind angle (relative to the dune toe) and dune slope inclination on the sediment transport patterns in coastal dunes. This knowledge can then be taken into account for design choices on slope inclination and orientation in artificial dunes. For example, to promote cross- or longshore sand transport where desired. Following this objective, some research questions have been formulated. The main research question is formulated as follows:

> What is the influence of the incident wind angle and slope inclination on the sediment transport patterns in coastal dunes?

To answer the main research question and to have a more structured research, several subquestions are set up. First of all, the influence of the incident wind angle and slope inclination to the flow patterns is investigated, to gain a better understanding of the flow that drives the sediment transport:

> 1. How do air flow patterns over a dune profile vary in relation to the incident wind angle and dune slope inclination?

Then, the influence of the two parameters on the sediment transport patterns is explored separately. Then, an answer to the main research question can be found by combining the answers to all subquestions. Therefore, the second subquestion is formulated as follows:

2. How does the incident wind angle impact the magnitude and direction of sediment transport at different parts of the dune?

Lastly, the third subquestion is formulated as follows:

3. How does the slope inclination impact the magnitude and direction of sediment transport at different parts of the dune?

## 1.3 Outline

An overview of relevant earlier research and the framework of this research is presented in Chapter 2. Subsequently, the methodology used in the research is shown in Chapter 3. After that, the results of the research are shown in Chapter 4. In Chapter 5, the results are discussed and limitations of the research are elaborated on. Finally, in Chapter 6, the final conclusions of the research are reviewed and recommendations are provided.

# 2 Literature review and framework

In this chapter, a review of previous research on the topics related to this research is reviewed. First, previous studies on air flow patterns are discussed. Secondly, the processes involved in and the prediction of aeolian sediment transport are presented. Third, the use of Computational Fluid Dynamics (CFD) in this field is discussed. Finally, the framework of this research in relation to Building with Nature projects in the Netherlands is presented.

## 2.1 Air flow patterns

The dynamics of air flow over aeolian landforms have been studied extensively over the past decades. In this section, some examples related to this research are shown. Research on topographic steering over beaches with foredunes show that winds approaching beaches at an oblique angle tend to be deflected towards crest-normal. This effect is greatest when the incident wind angles are between 30° and 60°, where 0° is cross-shore (e.g. Walker et al., 2009a). Moreover, significant onshore steering of near-surface sand transport vectors by as much as 37° from the incident wind angle was observed. In contrast, highly oblique winds with angles larger than 60° to the foredune crest can be deflected parallel to the beach. The degree of deflection depends on the incident wind angle as well as height above the surface. The most pronounced steering occurs near the surface and up steep slopes (e.g. Hesp et al., 2015). In general, flow acceleration on sloped surfaces tends to increase the shore-normal component of the flow vector for most oblique winds, whereas highly oblique winds are steered more alongshore.

In another study on the dynamics over steep dune slopes, Davidson et al. (2022) investigated flow dynamics over a high, unvegetated, and quite steep (30°) slope using field measurements. About halfway up the scarp, there is a change in slope, which causes some interesting, not previously shown dynamics to occur. Flow expansion at the change in slope caused a significant drop in wind speed on the upper slope segment. This is contrary to what has previously been found: the maximum percentage speed-up at the crest. For example, the widely used maximum speed-up formula at a dune crest by P. Jackson and Hunt (1975) is off by almost a factor of two. Moreover, an increase in turbulence was observed at the toe of the slope. This was followed by a gradual decrease in turbulence up-slope due to streamline convergence. This is frequently shown previously in wind flow studies over dunes. However, the change in slope and subsequent flow expansion that resulted in a decrease in wind speed also caused a significant increase in turbulence at the crest. In other dune studies the least degree of turbulence is typically found at the crest. All in all, this shows the importance of the shape of the dune on the flow patterns around it.

Dunes do not always have mild slopes and can potentially be quite steep, due to vegetation growth or scarping. Whereas with milder slopes complex flow patterns occur mostly on the lee side of the dune, with steep slopes flow separation can also be induced at the stoss slope. Relevant to dune formation following scarping and scarp fill processes, the formation of a separation region in front of a scarp will likely lead to the formation of an echo dune, as shown, for example, by Tsoar (1983).

## 2.2 Aeolian sediment transport

Understanding the process of air flow induced (aeolian) sediment transport, is an important step to better understand morphological changes occurring on sandy surfaces. First, a short overview of transport formulas will be presented, exhibiting the history of aeolian sediment transport in the scientific community. Thereafter, the focus will shift to limiting factors on aeolian sediment transport. Finally, the use of a process-based numerical model is summarized (AeoLiS), which can reproduce aeolian sediment transport and morphological changes in different coastal environments.

### 2.2.1 Transport formulas

There are many different known ways of sediment transport by wind (Figure 2). This makes capturing all aeolian sediment transport in one equation all the more difficult. Saltation is the most common form

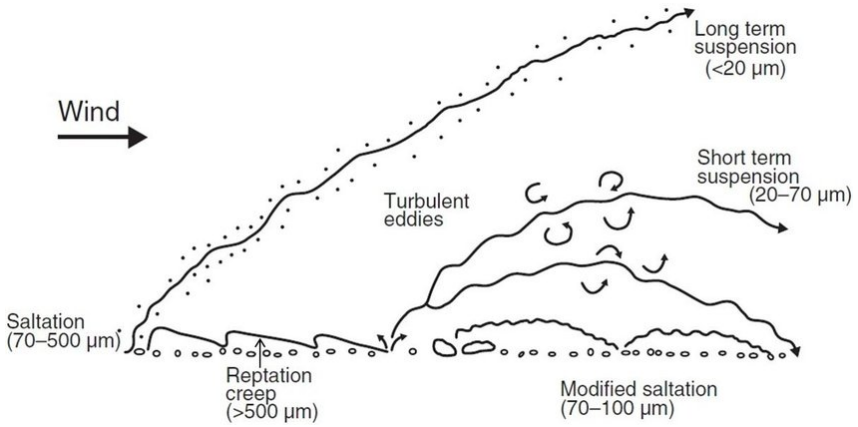


FIGURE 2: Different modes of aeolian sediment transport. Adopted from Nickling and Neuman (2009).

of aeolian transport on beaches, which occurs for sediment particles with a diameter of 70-500 $\mu$m. The research by Bagnold (1937) was the first to find some empirical relationship linking air flow above the surface to sediment transport on the surface. He found that sediment transport scales with the shear velocity to the third power. The shear velocity, however, is not easy to measure in reality. The logarithmic wall function was introduced by Richards and Hoxey (1993), relating the flow velocity at a height $z$ ($U(z)$) to the shear velocity $u_*$:

$$U(z) = \frac{u_*}{\kappa} \ln\left(\frac{z}{z_0}\right), \tag{1}$$

where $\kappa$ is the von Kármán parameter, and $z_0$ is the bed roughness length. Since then, this has been the favored method to derive the shear velocity, which is usually assumed to be constant with height above the surface.

However, research by Sherman et al. (1998) showed that there is a high uncertainty for calculating the shear velocity using the logarithmic wall function, and that it is only applicable where the vertical velocity profile is logarithmic, which is not in general the case over a dune profile (e.g. Hesp and Smyth, 2021).

Since the proposed transport formula by Bagnold (1937), many other transport formulas have been suggested. Besides difficulties with the calculation of the shear velocity, there has been much debate over the way the sediment transport scales to it. For example, Ho et al. (2011) proposed a quadratic scaling for erodible beds, Durán et al. (2011) proposed a quadratic scaling anywhere, and De Vries et al. (2014) proposed that for supply limited situations, a linear relation is better.

The development of the commonly-used sediment transport models has been covered comprehensively by other reviewers, and will not be repeated here (e.g. Dong et al., 2003; Kok et al., 2012; Walker, 2020). What is interesting to show here, is that these different formulas can give very large differences in sediment transport values, which is shown in Figure 3.

### 2.2.2 Limiting factors to aeolian sediment transport

There are some important limiting factors on aeolian sediment transport: sediment moisture, vegetation, sloping surfaces and supply limitations.

Soon after the first formula was proposed by Bagnold (1937), it was found that there is a threshold velocity, below which there is no sediment transport (e.g. Kawamura, 1951). The limiting capacity of sediment moisture, vegetation and sloping surfaces can be taken into account by adapting this threshold velocity.

The effect of moisture on sediment transport is usually incorporated by changing the threshold shear velocity with an empirical formula (e.g. Horikawa et al., 1982). In addition, the effect of vegetation on

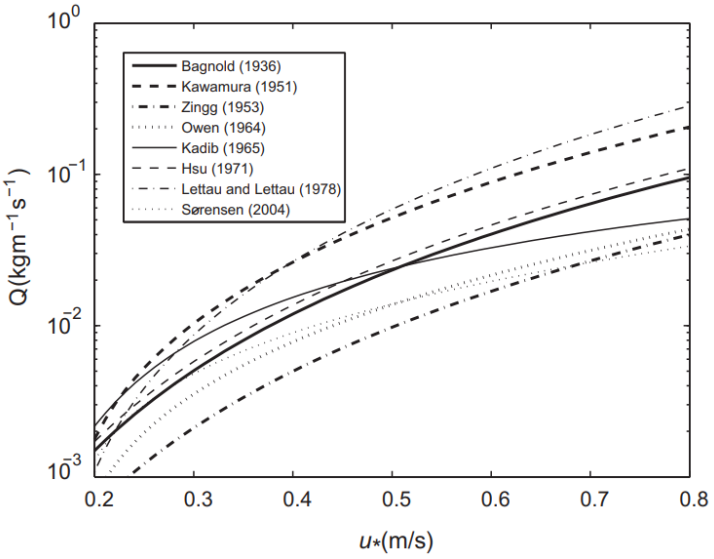


FIGURE 3: Sediment transport (Q) for different commonly-used sediment transport formulas (line styles). Adopted from Sherman and Li (2012).

sediment transport can also be incorporated by changing the shear velocity (e.g. Durán and Moore, 2013).

According to Sherman and Li (2012), unless local slopes exceed about 15°, the predicted effects of a slope on sediment transport rate are small. However, steeper slopes do occur in dune systems and can have a significant impact on the sediment transport. This is commonly done using either an adjustment directly to the sediment transport magnitude with the method by Bagnold (1973) (e.g. Sherman et al., 1998; Smyth and Hesp, 2015), or again by an adaptation of the threshold shear velocity with the method by Iversen and Rasmussen (1994) (e.g. Roelvink and Costas, 2019).

A transport equation where all the above limitations are taken into account is proposed by Strypsteen et al. (2019) and shows promising results: an accurate hindcast could be produced of the evolution of a part of the Belgian coast. However, a lot of specific on-site knowledge (sand composition, moisture content, wind data, etc.) and calibration with previously gathered data is generally needed to make it applicable for predicting sedimentation and erosion.

Supply limitations such as sediment sorting and armoring, air humidity and fetch length are also present in nature and can be taken into account, but are often difficult to incorporate well into a model.

### 2.2.3 AeoLiS

Although there are many ways to model aeolian sediment transport on beaches, AeoLiS will be highlighted here. AeoLiS is a process-based model for simulating aeolian sediment transport in situations where supply-limiting factors are important, such as in coastal environments. The model is open-source and its maintenance and development is done in a collaboration between multiple institutions: Deltares, the U.S. Army Engineer Research and Development Center (ERDC), Delft University of Technology and the Katholieke Universiteit Leuven. This model takes into account all of the limiting factors that were explained in section 2.2.2 and can simulate the morphological evolution of different coastal environments (Hoonhout and Vries, 2016). However, in terms of air flow modeling, which influences the sediment transport and morphological evolution, the model is limited and approximations are done to transform a wind flow above the surface to shear stresses/shear velocity at the surface. For example, in Cohn et al. (2019), the Coastal Dune Model (CDM, Durán and Moore, 2013) is used to handle the wind transformation towards a bed shear stress. Still, turbulent eddies or separation bubbles that can happen in coastal environments are not fully taken into account and a coupling with a CFD model could possibly lead to even better predictions.

## 2.3 CFD modeling

With the rapid increase of computational power over the past decades, numerical simulation has become increasingly prevalent. According to Smyth (2016), most studies nowadays use Computational Fluid Dynamics (CFD) to perform numerical simulations of near-surface flows. CFD is the process of mathematically modeling a physical phenomenon involving fluid flow and solving it numerically using computational power. Advantages of CFD include but are not limited to:

- Data can be measured at a very high resolution. In field studies and wind tunnel experiments, it is usually very difficult and/or expensive to measure things like wind flow, pressure, turbulence, and shear stress over the whole domain at a high resolution. However, with CFD, this is all given as an output for each grid point in the domain, even without disrupting the boundary flow conditions as you may in a wind tunnel or field experiment.
- Compared to other numerical methods, CFD gives the ability to resolve separation zones by solving turbulent nonlinear flow. This is important for many reasons, including the investigation of flow dynamics around aeolian landforms.
- CFD models can be easily adapted to fit the situation one wants to simulate. For example, boundary conditions such as wind speed, wind direction, and surface roughness can be quickly changed to test a variety of hypotheses.

The most notable disadvantage of CFD modeling is the fact that assumptions always need to be made (e.g. flow models, parameter settings, simplified boundary conditions), which inevitably leads to errors. Also, when very detailed results are needed, or the computational domain is very large, computational time can be too long to do multiple relevant simulations.

### 2.3.1 Solving Navier-Stokes

In the case of air flow, the Navier-Stokes equations are usually solved to give insight in the flow patterns. These equations are a set of complicated partial differential equations and with the use of numerical methods, these equations can be solved with increasing accuracy. Three ways are most common to do this, namely by Direct Numerical Simulation (DNS), Large Eddy Simulation (LES) and Reynolds-Averaged Navier-Stokes (RANS). The difference lies in the way the turbulence is modelled. With DNS, the equations are attempted to be solved over all turbulent scales. This means that you need a very high resolution everywhere in your computational domain, which is computationally costly. Secondly, with LES, only the larger turbulence scales are resolved, which remains a computationally expensive task for larger domains, though it is a lot cheaper than DNS. Lastly, with RANS, all flow velocities are calculated as average values, and the turbulence (or the fluctuations around those average flow velocities) is resolved using Reynolds stresses and a turbulence closure model. According to Smyth (2016), there have been only a few studies in aeolian landforms using the LES approach, against a large number of RANS simulations. However, with increasing computational power, it is expected that LES will obtain more attention in future studies.

### 2.3.2 CFD studies: Air flow patterns

Many studies have used CFD to model air flow patterns over a slope. In one of the first uses of CFD in the field of dunes by Parsons et al. (2004), a 2D model was developed using the PHOENICS 3.5 software to simulate the streamwise and vertical velocity flow fields over small-scale, idealized transverse dunes of varying height and stoss slope basal length. Results indicate that the flow field over transverse dunes is particularly sensitive to changes in dune height. An increase in height causes a flow deceleration at the toe, streamwise acceleration and vertical lift at the crest. In addition, the higher the dune is, the larger the extent of the lee-side separation cell, and the stronger are the reversed flows within. High correlation coefficients were found comparing the model to wind tunnel data of Walker and Nickling (2003).

In the study by Hesp and Smyth (2021), wind flow over a 2 m high scarp with varying slope angles (45°, 24°, and 14°), three vertical slopes of differing heights (1 m, 2 m and 4 m) and a 2 m vertical slope subjected to three oblique incident wind angles was investigated. For winds perpendicular to the dunes, they found no flow separation at the base of the slopes, or downwind of the crest on the lower slopes (45° and less).

### 2.3.3 CFD studies: Sediment transport

In a study by Smyth and Hesp (2015), air flows over three different (artificial) sand ridges on the beach were simulated with the use of CFD. With the transport formula by Lettau and Lettau (1978) and the slope correction by Bagnold (1973), they also give an indication on the sediment transport over the structure. They qualitatively found that steeper stoss slopes led to an increased reduction in shear velocity at the toe of these scarp-like structures, and this resulted in greater sediment deposition aiding in foredune recovery.

As mentioned before, the shear velocity is usually calculated using the logarithmic wall function (Equation 1), as the shear velocity is difficult to measure. However, a more accurate method can be applied when using a CFD model by calculating the shear velocity directly from the bed shear stresses. The bed shear stresses, $\vec{\tau}$, can generally be extracted from the simulation results of a CFD model. Subsequently, the shear velocity can be established by $|\vec{\tau}| = \rho u_*^2$, which eliminates inaccuracies for $u_*$ that occur by the use of the wall function (Smith et al., 2017a).

### 2.3.4 CFD studies: an overview

Table 1 shows an overview of a selection of studies that have used CFD to model air flow patterns and/or sediment transport in aeolian environments. A few things can be hypothesized from this table:

- Three-dimensional modeling is more common in recent years.
- The RNG $k-\epsilon$ turbulence closure model is the most common, followed by the $k-\epsilon$ turbulence closure model.
- Nowadays, OpenFOAM is most commonly used to do CFD modeling of air flow patterns.
- The SIMPLE method to solve the RANS equations is the most common.

TABLE 1: A selection of studies using CFD to model air flow, including dimensions, turbulence closure model, software, numerical solution method, how shear velocity is calculated, and the number of cells or grid resolution.

| *Study* | *2D/3D* | *Turbulence* | *Software (method)* | *Shear velocity calculation* | *Number of cells* |
|---|---|---|---|---|---|
| Pourteimouri et al., 2022 | 3D | $k-\epsilon$ | OpenFOAM (SIMPLE) | From log profile, Richards and Hoxey (1993) | $4.57 \cdot 10^7$ |
| Hesp and Smyth, 2021 | 3D | RNG $k-\epsilon$ | OpenFOAM (SIMPLE) | From log profile, Richards and Hoxey (1993) | Unknown, mesh resolution of 0.2 m |
| Smith et al., 2017b | 3D | $k-\epsilon$ | OpenFOAM (unknown) | Direct calculation from shear stress | $2 \cdot 10^7$ |
| Smith et al., 2017a | 3D | $k-\epsilon$ and RNG $k-\epsilon$ | OpenFOAM (unknown) | Direct calculation from shear stress | $3.9 \cdot 10^6$ |
| Hesp and Smyth, 2016 | 2D | RNG $k-\epsilon$ | OpenFOAM (SIMPLE) | From log profile, Richards and Hoxey (1993) | Unknown, hor. res. 0.25 m and vert. res. 0.1-1.63 m |
| Smyth and Hesp, 2015 | 3D | RNG $k-\epsilon$ | OpenFOAM (PIMPLE) | Direct calculation from shear stress | $2.5 \cdot 10^6$ |
| Araújo et al., 2013 | 2D | RNG $k-\epsilon$ | FLUENT (SIMPLE) | No calculation | Unknown, mesh resolution of 0.05 m |
| D. Jackson et al., 2013 | 3D | RNG $k-\epsilon$ | OpenFOAM (PIMPLE) | Unknown | $2 \cdot 10^6$ |
| Parsons et al., 2004 | 2D | RNG $k-\epsilon$ | PHOENICS 3.5 (SIMPLEST) | Unknown | Unknown |

## 2.4 Framework

In this section, the framework of this research in relation to Building with Nature projects in the Netherlands is shown. First, the ShoreScape project and how this research is related to it is explained. After that, the conclusions from the Hondsbossche Dunes project that are most relevant to this research are presented.

### 2.4.1 ShoreScape

In 2017, after receiving a grant from the Netherlands Organisation for Scientific Research (NWO), the ShoreScape project started. The title of the project reads: Sustainable co-evolution of the natural and built environment along sandy shores. The overall goal of the project is to develop the knowledge, tools and design principles for a dynamic occupation of the land-sea interface to enhance 'building with nature' (BwN) processes and contribute to the natural adaptation and durable development of urban coastal zones along sandy shores. In other words: How can we design a coastline, using knowledge on aeolian sediment transport, such that the design contributes to both the sustainability, ecology and recreation? For example, where is it most beneficial for sediment to accumulate/erode, and to what extent can we influence this?

Multiple researchers are affiliated with ShoreScape and have contributed to this goal. Poppema et al. (2018) investigated the effect of building orientation and dimensions on the sedimentation and erosion patterns around buildings on the beach through field experiments. Van Bergen et al. (2020) did research on different spatial interventions to enhance dune formations after a shore nourishment. This was done by looking at different case studies and focuses on spatial beach design. Research by Pourteimouri et al. (2022) focuses on aeolian sediment transport patterns around buildings in terms of physical processes. Using CFD, the air flow around buildings on a beach was simulated. From the results, a better understanding of the sediment transport and erosion and sedimentation patterns was gained.

In line with the research by Pourteimouri et al. (2022), this thesis focuses on the use of CFD to gain a better understanding of the physical processes regarding sediment transport that occur in a beach-dune system. Answering the main research question leads to a better understanding of where sedimentation or erosion can be expected, related to the obliqueness of the dune toe and the slope inclination of a dune.

### 2.4.2 Hondsbossche Dunes

From the start of 2014 until December 2015, 35.6 $Mm^3$ of sand was placed in front of the Hondsbossche and Pettemer Zeewering (HPZ). The new beach-dune system that had been created with this operation was afterwards called the Hondsbossche Dunes. This was done to provide a reinforcement to a weak part in the sea defense, using the Building with Nature approach. This innovation project was called EcoShape HPZ and was done as a collaboration between multiple companies and knowledge institutes.

The location of the Hondsbossche Dunes ('studiegebied'), the HPZ and the location of different dune profile types ('Profieltype') is shown in Figure 4.

The gathered data from the Hondsbossche Dunes promises to be a valuable source of information to compare simulation results with. In the report by Bodde et al. (2019), conclusions are drawn and ideas are proposed, related to sediment transport patterns in a(n) (artificial) dune system. These claims can be compared to model simulation results to support or oppose them, wherever this is possible.

Two conclusions from the project will be highlighted here: one on the influence of dune toe orientation, and one on the sedimentation pattern over the dune profile.

### 2.4.3 Sediment deposition pattern at Hondsbossche Dunes

The overall sediment deposition pattern that was measured was different than predicted. They found that on average, approximately 70% of the accumulated sand in the dune area was captured in the area around the dune toe and on the dune slope below 8 m+NAP, and 25-30% in the area 10-30 m landward from the dune crest (Figure 5). In advance, it was expected to see more sediment transport further landward of the dune top, but only a very small percentage ended up there (0-5%). This sedimentation pattern was also

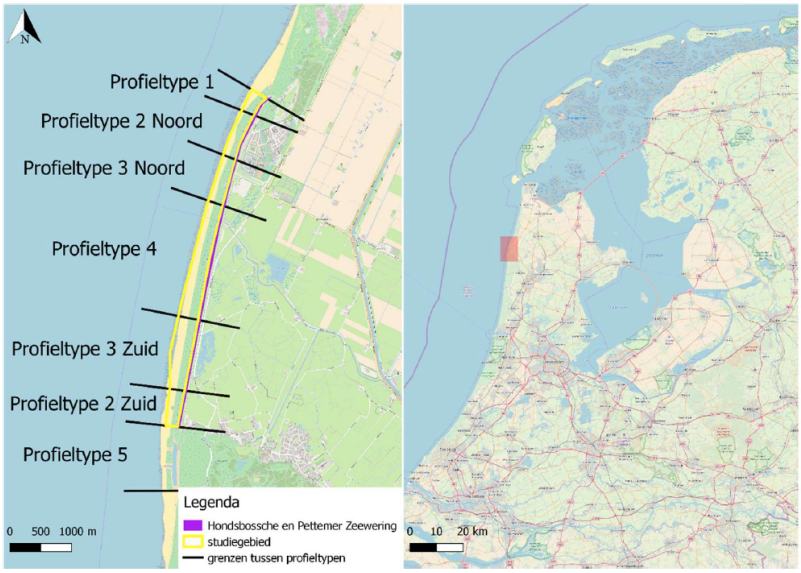


FIGURE 4: Overview study area of the Hondsbossche Dunes, including different dune profile type locations. Adopted from Bodde et al. (2018).

quite similar between the different dune profiles, only the distribution of sand on the seaward side of the dune varied.

### 2.4.4 Influence of dune toe orientation at Hondsbossche Dunes

Figure 6 shows the differences in sedimentation for the different dune profiles in boxplots. The focus here will be on the results of dune profile type 2 (highlighted boxes). Although the two dune profiles of type 2 — north (P2N) and south (P2Z) — were initially the same, a large difference in sedimentation on the dune was measured (Figure 6). This difference in sedimentation is quite large: in the north, only about 15 $m^3$/m/year of sedimentation is found, and in the south, 30 $m^3$/m/year. Figure 7 shows the evolution of two cross-sections in the study area, one P2N and one from P2Z. Clearly, much more sedimentation occurs on P2Z, especially on the dune slope. Moreover, Figure 7A shows that sedimentation occurs in particular around the sand trapping fences ('wilgenscherm').

The differences in sedimentation were attributed to the difference in dune toe orientation (Figure 4). Namely, an average dune toe orientation of 282° and 295° was found for the southern and the northern type 2 profile, respectively (Bodde et al., 2018). Consequently, from these results it is hypothesized that a difference of 13° in wind incidence (from 282° to 295°) can lead to an increase in sedimentation on the dune from 15 $m^3$/m/year to 30 $m^3$/m/year.

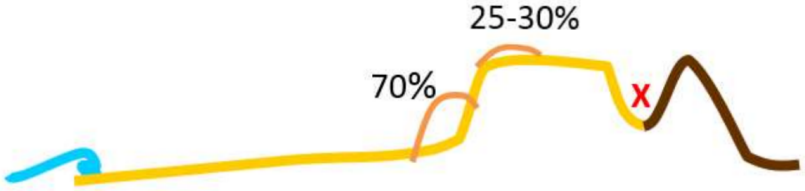


FIGURE 5: Schematization of the measured sediment deposition pattern in the Hondsbossche Dunes. Adapted from Bodde et al. (2019).

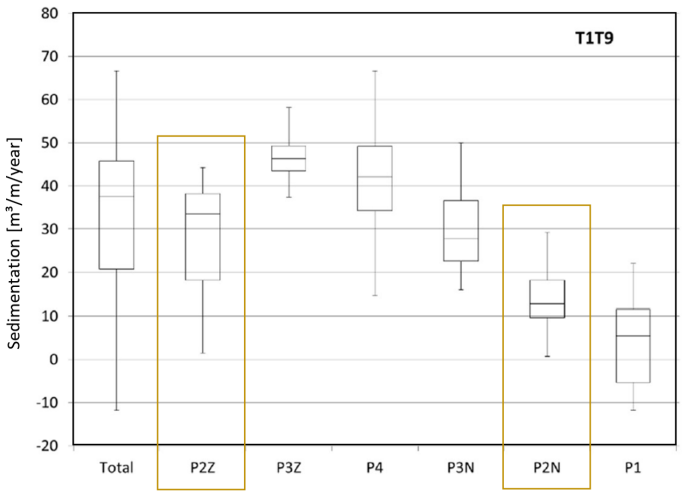


FIGURE 6: Boxplots with minimum, 25%, 50%, 75% and maximum value of sedimentation in the dune in $m^3$/m/year between T1 (05-2015) and T9 (03-2018) per dune profile type. The results from the southern (P2Z) and northern (P2N) type 2 dune profile are highlighted. Adapted from Bodde et al. (2018).

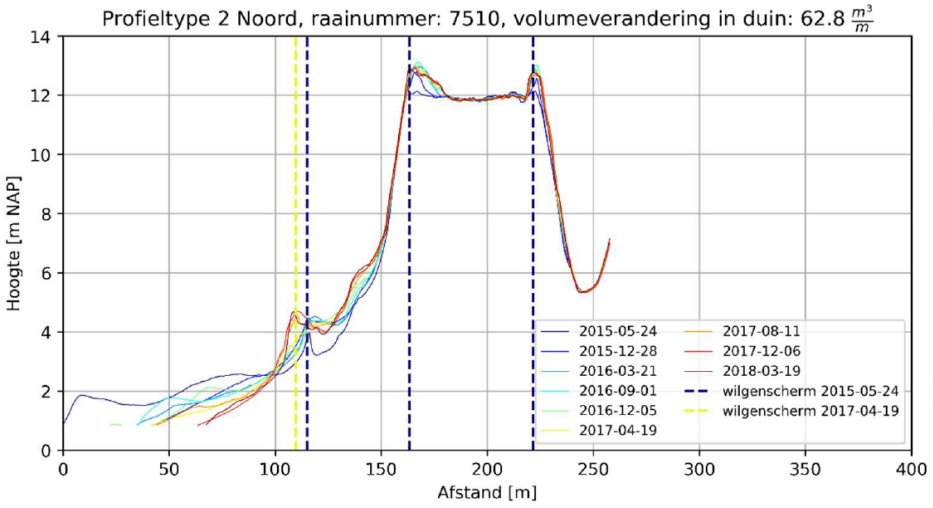


(A)

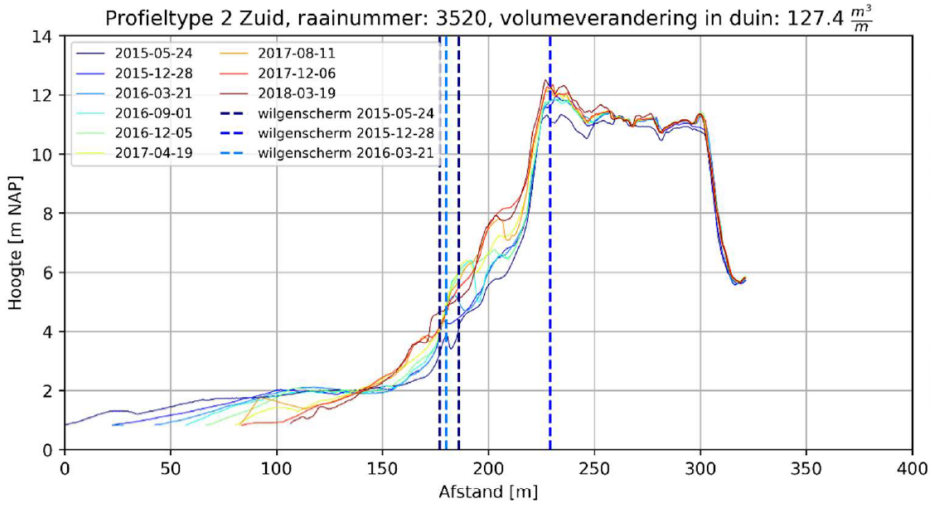


(B)

FIGURE 7: Dune profile type 2 development with multiple locations of a sand trapping fence ('wilgenscherm'). Adopted from Bodde et al. (2018). (A) Northern type 2 dune profile (P2N). (B) Southern type 2 dune profile (P2Z).

# 3 Methodology

In this chapter, multiple facets of the methodology will be discussed. First of all, the model setup with all relevant components is shown. Secondly, the decisions made regarding the variation in incident wind angle and slope inclination are discussed. Next, the details on the calculation of aeolian sediment transport and morphological change are explained. Lastly, the iterative process used in this research is shown.

## 3.1 Model setup

To answer the research questions, simulations have been done using a CFD model. A number of things are needed in order to perform accurate simulations with such a model:

- Solver
- Model domain
- Computational grid
- Boundary conditions

### 3.1.1 Solver

To answer the research questions, simulations are performed with the open source CFD software OpenFOAM. The SIMPLE (Semi-Implicit Method for Pressure Linked Equations) algorithm is used to solve the Reynolds-Averaged Navier-Stokes equations (Patankar and Spalding, 1983). Simulations were considered sufficiently converged once the initial residual of an iteration was less than $10^{-5}$ m/s for the velocities in $x$-, $y$- and $z$-direction. Subsequently, a steady-state, Reynolds-averaged solution of the flow over the domain is obtained. More numerical simulation settings are specified in Appendix C.1.

### 3.1.2 Model domain

The model domain is roughly derived from the dimensions of dune profile type 2 of the Hondsbossche Dunes (Bodde et al., 2019, Figure 7). This was done for three reasons. First of all, the project of the Hondsbossche Dunes is well-documented, including design processes and monitoring of the morphological changes after construction, which allows for comparison between model and field results. Secondly, profile type 2 was used because of the relative simplicity of the profile, without any valley or smaller dune between the main dune and the sea. Lastly, this domain was chosen because of the collaboration with employees of Witteveen+Bos, who have worked on the EcoShape project of the Hondsbossche Dunes and could explain more details if needed during the research.
This leads to the following dimensions:

- Beach width of 150 m
- Dune toe at 3 m+NAP
- Dune top at 10 m+NAP
- Dune top width of 50 m

Looking at these dimensions and the fact that a longshore uniform model will be used, one might say that a 2D model is enough for doing this research. While this might be reasonable for some applications, in this case a 3D model is needed to also allow for investigating changes of wind direction and therefore transport direction over the beach-dune system. A short longshore beach length is already enough to include these effects. This allows for a fine mesh size in longshore direction, while not having too many grid cells over the whole domain. A schematized view of this setup is shown in Figure 8, where $\theta$ is defined as the incident wind angle, relative to the line normal to the dune toe. Moreover, the dune slope is subject to change between the different simulations. Consequently, since the dune height is kept constant, the cross-shore width of the dune slope varies.

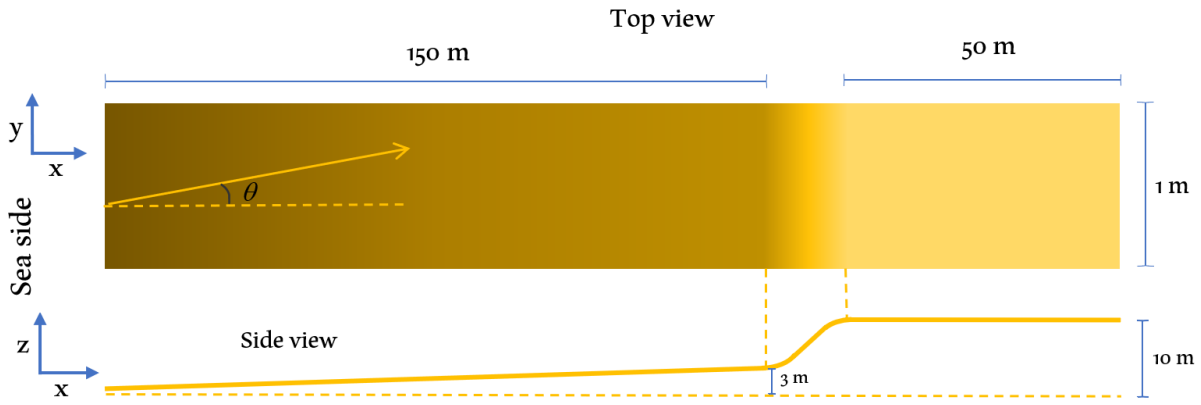


FIGURE 8: Schematization of the computational domain.

### 3.1.3 Computational grid

With the model domain defined, the computational grid can be formed. This is done using the `blockMesh` dictionary, such that the grid is systematically generated for each simulation and can be reproduced exactly (Appendix C.2). For the general testing of grid cell size (Appendix B.1), the influence of the domain depth (Appendix B.2) and the reference wind speed at the inlet (Appendix A.1), a dune shape with straight lines and sharp edges was used (Appendix A.2). The rest of the simulations are done using a more natural dune shape, where the changes in slope at the dune toe and dune top are smoothed. This is done with the aim to eliminate the influence of the steep gradients in flow velocity and pressure at those locations. The smoothing is done in the following way. Points A and D in Figure 9 define the beginning and the end of the dune slope, respectively. A straight line between points B and C is drawn, where B and C are the points at respectively $\frac{1}{5}$th and $\frac{4}{5}$th of the total cross-shore dune slope width (Figure 9). The slope of this line defines the dune slope inclination ($\gamma$). Then, the connection arcs are defined by a smooth curve, such that the slope derivative over the entire dune profile is continuous.

Subsequently, more natural simulation results are found, because completely sharp edges are usually

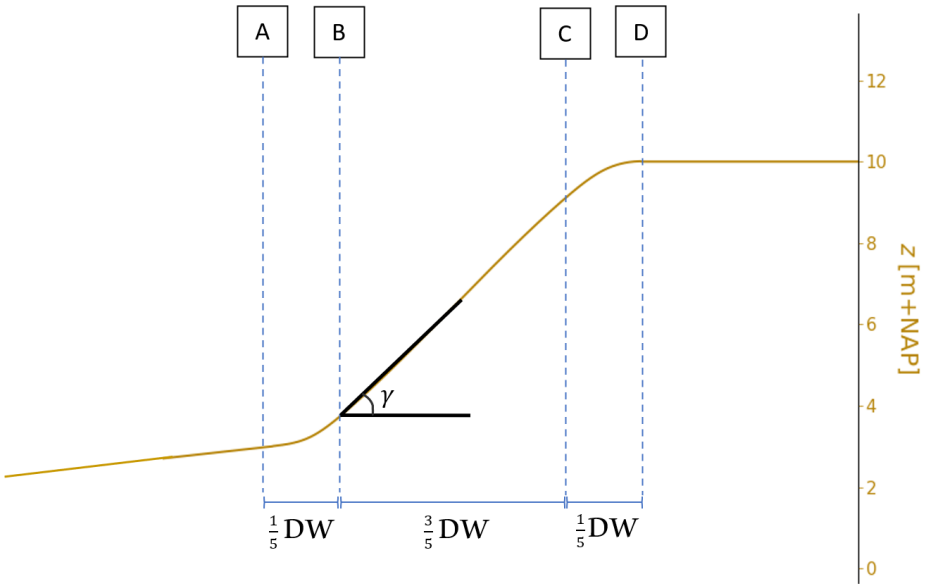


FIGURE 9: Illustration of the smoothing procedure of the slope from the dune toe to the dune crest. DW (Dune Width) denotes the distance from the dune toe at 3 m+NAP (point A) to the dune crest at 10 m+NAP (point D).

not present on dunes or steep slopes in nature. The difference in simulation results is further explored in Appendix A.2. In terms of grid cell size, multiple tests were done to determine which cell size to use. For further elaboration on this topic, the reader is referred to Appendix B.1. In the end, it was decided to use the following minimum grid cell dimensions: $\Delta x = 0.15$ m, $\Delta y = 0.1$ m, $\Delta z = 0.1$ m. These dimensions were used in the area on and around the dune slope, which contains the largest changes in flow velocity and direction. An example of the grid, with a dune slope of 40°, is shown in Figure 10, showing how the grid cells become larger further away from the surface and away from the dune slope. Lastly, the height and depth of the computational domain are set at 50 m and 1 m, respectively. The total number of grid cells per simulation is shown in Table 2.

### 3.1.4 Boundary conditions

An atmospheric boundary layer (ABL) model is used to define the vertical profiles of wind speed ($U$), turbulent kinetic energy ($k$) and energy dissipation ($\epsilon$) at the inlet boundary. This is done using built-in OpenFOAM functions, which assume a constant shear velocity ($u_*$) value with height (Blocken et al., 2007; Richards and Hoxey, 1993).

A parameter that influences the ABL and must be specified for the definition of the vertical profiles at the inlet boundary, is the roughness length of the bed ($z_0$). In the simulations, this value was set to

TABLE 2: Settings for the different performed simulations, including the number of grid cells per slope variation.

| Dune slope inclination / $\gamma$ [°] | Incident wind angle / $\theta$ [°] | | | | | | Number of grid cells |
|---|---|---|---|---|---|---|---|
| 10 | 0 | 15 | 30 | 45 | 60 | 75 | 617600 |
| 20 | " | " | " | " | " | " | 486400 |
| 30 | " | " | " | " | " | " | 444800 |
| 40 | " | " | " | " | " | " | 427200 |
| 50 | " | " | " | " | " | " | 419200 |
| 60 | " | " | " | " | " | " | 418400 |
| 70 | " | " | " | " | " | " | 428000 |
| 80 | " | " | " | " | " | " | 462400 |

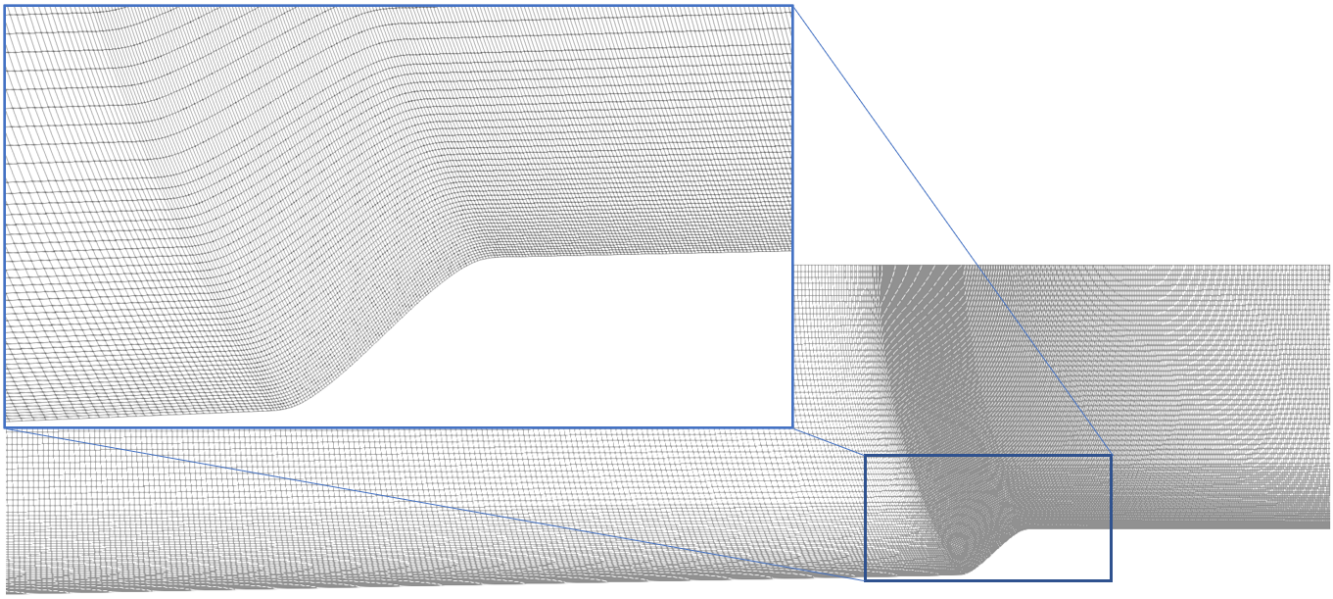

FIGURE 10: Side view of the computational grid used in the CFD model ($\gamma = 40°$). The highlighted box shows a close-up of the slope.

$z_0 = 0.0001$ m. This is a low estimate of the roughness length for smooth, sandy surfaces (Troen and Petersen, 1989). However, this value is generally difficult to measure and is often calibrated using field data. More on the impact of this choice is explored in section 4.4.3.

A reference flow velocity of 20 m/s is used at a height of 1.8 m above the surface. More explanation on this choice and the influence of the wind speed can be found in Appendix A.1. The lateral boundaries of the computational domain are defined as cyclic boundaries, to assure that the flow conditions are periodically repeating between these two boundaries. This is reasonable to do for a longshore uniform domain. The bottom patch is defined as a no-slip boundary, while the top patch is defined as a slip boundary. The outlet of the domain is set to have no gradient for each of the parameters.

The incident wind angle is defined by setting the value for flow direction at the inlet to $\cos(\theta)$ and $\sin(\theta)$ for the cross-shore and longshore direction, respectively.

## 3.2 Incident wind angles and dune slopes

In order to obtain a better understanding of the influence of wind direction on flow patterns and sediment transport, the angle at which the flow enters the model domain is varied. Although there are some exceptions in terms of location, winds at the coast are predominantly landward winds. Also, winds that come from the land are often less strong and therefore do not have a large impact on the sediment transport over the dune. For example, the wind rose from the study by De Winter et al. (2020) shows the wind conditions at the IJmuiden weather station, confirming these statements for a large part of the Dutch coastline (Figure 11). The figure also shows the dune toe orientation at the Hondsbossche Dunes of the northern and southern type 2 dune profile (P2N and P2Z, respectively). With a dominant wind direction of 225° (Bodde et al., 2018, agreeing with the dominant wind direction at IJmuiden), this means that on the southern part, the dominant incident wind angle relative to the dune toe equals 57°, and in the northern part it equals 70°.

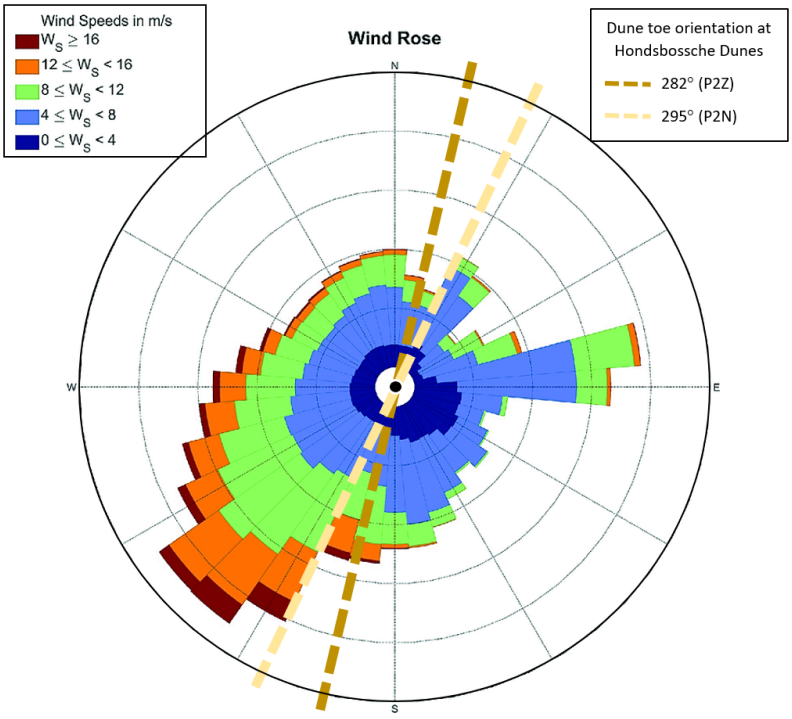


FIGURE 11: Wind rose at the IJmuiden weather station based on 10-minute data from January 1, 2007 up to and including December 31, 2016. The dashed line denotes a dune toe orientation of 285°. Adapted from De Winter et al. (2020).

Moreover, since the model domain is longshore uniform, a negative incident wind angle gives the same simulation results as an equal but positive incident wind angle, albeit mirrored. Therefore, the performed simulations have an incident wind angle varying from 0° to 75°, with steps of 15°. Consequently, this gives 6 different simulations per dune slope (Table 2).

Furthermore, in order to obtain a better understanding of the influence of the dune slope on flow patterns and sediment transport, the dune slope of the model domain is varied. Coastal dunes in nature generally contain windward (stoss) slopes of 15°-30°. This is also approximately the range in dune slope inclinations implemented at the Hondsbossche Dunes (Bodde et al., 2019). However, due to scarping, often higher slopes can be found as well. These scarps can either gradually become less steep due to slumping or erosion events, or stay present due to the presence of roots of dune vegetation that keep the sand together. Therefore, the performed simulations have a dune slope varying from 10° to 80°, with steps of 10°. This results in 8 different simulations per wind angle. In conclusion, a total of 48 simulations were performed to obtain relevant results (Table 2).

## 3.3 Aeolian sediment transport and morphological change

In this section, the equations involved in the calculation of aeolian sediment transport and morphological change are discussed.

### 3.3.1 Aeolian sediment transport

For the analysis of aeolian sediment transport, the extracted bed shear stresses in cross-shore, longshore and vertical direction ($\tau_x$, $\tau_y$ and $\tau_z$, respectively) are used. The magnitude of the bed shear stress ($|\vec{\tau}|$) is first calculated, after which the shear velocity magnitude ($u_*$) can be found with the following equation:

$$u_* = \sqrt{|\vec{\tau}|/\rho_a}, \tag{2}$$

where $\rho_a$ denotes the density of air. The value used for the density of air is $\rho_a = 1.293$ kg/m$^3$, which is the density of air at standard atmospheric pressure at 0 °C (Engineers Edge LLC, 2000). From there, the Bagnold sediment transport formula is used to calculate the sediment transport magnitude ($q$) in kg/m/s (Bagnold, 1937):

$$q = C \cdot \left(\frac{\rho_a}{g}\right) \cdot \sqrt{\frac{d}{D}} \cdot (u_* - u_{*,\mathrm{th}})^3, \tag{3}$$

where $C$ is a constant, $d$ is the mean grain diameter for the sand, $D$ is a reference grain diameter, and $u_{*,\mathrm{th}}$ is the threshold shear velocity for sediment transport. The constant $C$ is chosen to be 1.8, as is common for naturally graded sand (Nickling and Neuman, 2009). The value of $D$ is set at 240 $\mu$m (Bagnold, 1937). The mean grain diameter ($d$) is chosen to be 300 $\mu$m, based on Bodde et al. (2019).

From $q$, the cross- and longshore sediment transport can be found:

$$q_x = q \cdot \frac{\tau_x}{|\vec{\tau}|}, \quad q_y = q \cdot \frac{\tau_y}{|\vec{\tau}|}. \tag{4}$$

In the sediment transport figures in this report, the sediment transport values are converted to a value in m$^3$/m/month to make a comparison easier to field data from the Hondsbossche Dunes. Since the simulations are done with a wind speed of 20 m/s, it is expected that the value per month is close to the value per year when the wind speeds are generally lower throughout the year (Figure 11).

The threshold flow velocity on a flat bed ($u_{*,\mathrm{th},0}$) is calculated with

$$u_{*,\mathrm{th},0} = A \cdot \sqrt{\frac{\rho_s - \rho_a}{\rho_a} \cdot g \cdot d}, \tag{5}$$

where $A$ is another constant (with value 0.1) and $\rho_s$ denotes the sediment density, which is set to be 2650 kg/m$^3$.

Since it is more difficult for sediment particles to travel upwards on sloping surfaces, an adjustment needs to be applied for sediment transport on a dune slope. The method by Iversen and Rasmussen (1994) adjusts the threshold shear velocity, which naturally influences the sediment transport (e.g. Roelvink and Costas, 2019). The adjustment is calculated as follows:

$$\frac{u_{*,\mathrm{th}}^2}{u_{*,\mathrm{th},0}^2} = \cos(\gamma_{\mathrm{rel}}) + \frac{\sin(\gamma_{\mathrm{rel}})}{\tan(\alpha)}, \tag{6}$$

where $\alpha$ is the sediment friction angle (34°) and $\gamma_{\mathrm{rel}}$ denotes the slope inclination relative to the direction of sediment transport, which varies depending on the cross-shore position ($x$). This relative slope angle can be calculated in the following way:

$$\tan(\gamma_{\mathrm{rel}}) = \frac{\partial z_b}{\partial x}\cos(\theta_\tau), \tag{7}$$

where $\theta_\tau$ denotes the direction of shear stress and thus sediment transport at the bed in the horizontal plane:

$$\tan(\theta_\tau) = \frac{\tau_y}{\tau_x}. \tag{8}$$

### 3.3.2 Morphological change

A common equation to determine morphological change due to sediment transport is found in the Exner equation:

$$\frac{\partial z_b}{\partial t} + \frac{1}{(1-n)\rho_s}\left(\frac{\partial q_x}{\partial x} + \frac{\partial q_y}{\partial y}\right) = 0, \tag{9}$$

where $z_b$ defines the surface level and $n$ is the porosity of the sand. The value of $n$ is chosen to be 0.4. The simulations result in Reynolds-averaged solutions, which means we do not have a time-varying $q_x$ and $q_y$. Therefore, the change in surface level is calculated, using discretization of the time derivative with a time step $\Delta t$, assuming constant sediment transport over this time step. However, in nature, the changes in morphology would lead to changes in sediment transport and a discretization therefore leads to a rough estimate of actual morphological changes. As a final step, we notice that the change in longshore direction equals 0 because of the longshore invariability of the domain. This means we can find the updated bed profile using the following equation:

$$\frac{z_{b,\text{updated}} - z_b}{\Delta t} + \frac{1}{(1-n)\rho_s}\frac{\partial q_x}{\partial x} = 0 \tag{10}$$

$$\Rightarrow z_{b,\text{updated}} = z_b - \Delta t \frac{1}{(1-n)\rho_s}\frac{\partial q_x}{\partial x}. \tag{11}$$

Another way to calculate sedimentation or erosion is by calculating the cross-shore sediment transport at one location, and subtracting the cross-shore sediment transport at a location further landwards. This results in the net cross-shore sediment transport over a specific area (from the first to the second location), showing accumulation or erosion in that area. This method will be used to calculate the net transport into the area in front of the dune slope (section 4.3).

## 3.4 Iterative process

The approach used in this research to perform multiple simulations can be visualized as an ongoing process (Figure 12). Starting with the generation of a computational grid with the right dune slope inclination, a simulation can be run. Following this, the flow velocity in all directions and the bed shear stresses can be extracted, which leads to the possibility of visualizing and analyzing the simulation results. Therefore, for each flow simulation, two data sets are produced: one containing the flow velocity values

($U_x$, $U_y$, $U_z$) and the other containing the shear stresses at the surface ($\tau_x$, $\tau_y$, $\tau_z$). The choice was made to use the flow velocity at 25 cm above the surface. This choice is somewhat arbitrary, but a distance close to the surface is chosen because it is then close enough to the surface to also represent the flow of sediment transport. Finally, for the next simulation, either the incident wind angle ($\theta$) is modified, after which the solver algorithm can be run again directly, or the dune slope inclination ($\gamma$) is changed, which requires a new grid generation.

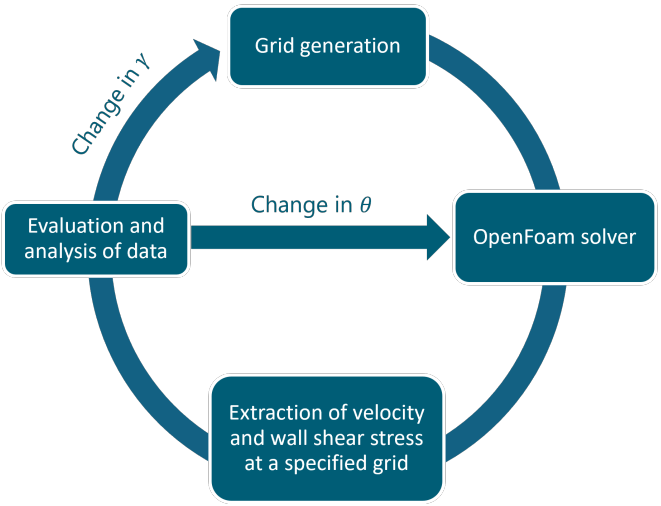


FIGURE 12: Steps in the main iterative process employed in this research: from the generation of a computational grid, to the analysis of the simulation results.

# 4 Results

The results from the simulations described in the methodology are presented in this chapter. The results will be shown on flow patterns, aeolian sediment transport and morphological change for dunes with different slope inclinations and under different wind directions. As a reminder: all flow velocities and wind directions displayed in this chapter are the simulated air flow velocities at 25 cm above the surface. As a general remark: In every figure showing a cross-shore variation over the domain, two vertical dashed lines denote the beginning and end of the dune slope.

## 4.1 Flow patterns

In this section, the change in flow patterns over the dune profile due to changes in incident wind angle and dune slope is shown.

### 4.1.1 Impact of incident wind angle on flow patterns

Figure 13 shows the flow velocity over the dune profile for a dune slope inclination of 30° and different incident wind angles (0°-75°). There is clearly a velocity decrease at the dune toe and speed-up over the dune slope. The flow velocity is lowest just before the point where the slope becomes 30°. Moreover, just before the dune crest, the flow velocity is highest. Upon a closer look, it can be seen that the peak velocity moves towards the dune top for higher incident wind angles. Furthermore, on the dune top, the velocity steadily decreases towards a base value, where more shore-normal angles show a higher base value. This will be further explored in section 4.4.2. Also, the least and the most change in flow velocity magnitude is seen for high and for low incident wind angles, respectively. Lastly, the changes in velocity are largest between incident wind angles of 30°-60°.

The change in flow direction for a slope inclination of 30° and different wind angles is shown in Figure 14A. For an incident wind angle of 0°, there is no flow reversal (because the flow stays attached to the surface for this slope inclination) or deflection (since the dune profile is completely longshore uniform), and hence there is no change in wind direction. For all other incident wind angles, we see:

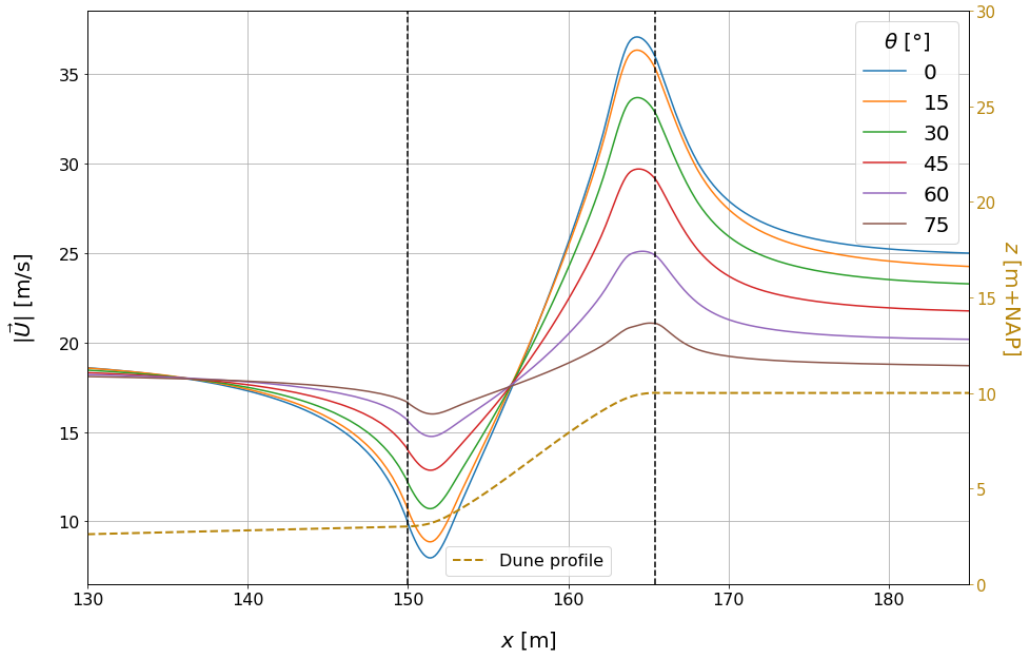


FIGURE 13: Change in magnitude of the flow velocity ($|\vec{U}|$, 25 cm above the surface) for a dune slope inclination of 30° and different incident wind angles (solid line colors).

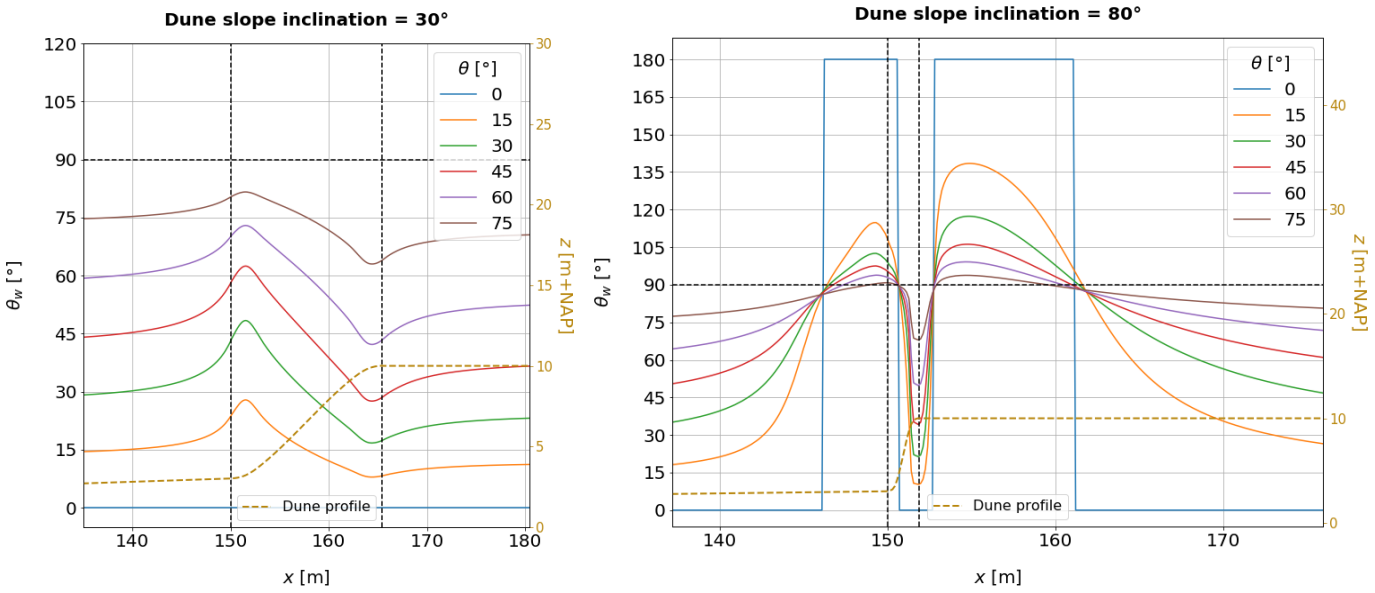


(A) (B)

FIGURE 14: Change in flow direction ($\theta_w$, 25 cm above the surface) for different incident wind angles (solid line colors). (A) Dune slope of 30°. (B) Dune slope of 80°.

- Longshore deflection at the dune toe.
- Stronger deflection towards a cross-shore flow over the dune slope.
- Return towards initial flow direction at the dune top.
- Strongest deflection for incident wind angles of 30°-60°.

These patterns are the same for lower slope inclinations, yet for steeper slopes, flow reversal can occur at the dune toe and on the dune crest (Figure 14B).
These results are in line with other studies investigating flow patterns over dunes, and therefore validate the use of the model for further research (e.g. Hesp et al., 2015; Tsoar, 1983; Walker et al., 2009b).

### 4.1.2 Impact of dune slope inclination on flow patterns

The change in cross-shore flow velocity over the dune profile for an incident wind angle of 0° and the different dune slope inclinations (0°-80°) is shown in Figure 15. The cross-shore flow velocity is shown, because for steep slopes, flow reversal at the dune toe and on the dune top occurs and therefore requires negative flow velocity values to show the flow pattern in the best way. Moreover, since the incident wind angle is 0°, there is no flow velocity in longshore direction, so $|U_x| = |\vec{U}|$ in this case.
Since the cross-shore length of the dune slope changes with differences in dune slope inclination, the cross-shore dune slope width ($DW$) is normalized. Therefore, the coordinate on the dune slope is denoted by $x^* := (x - 150)/DW$. Since the dune top is equal in width for all dune slope inclinations, the coordinate for that section is denoted with $x - x_{crest}$, where $x_{crest}$ represents the $x$-value at the dune crest.
Figure 15 shows the differences in cross-shore flow velocity for changes in dune slope inclination. Clearly, the velocity at the dune toe steadily decreases for steeper slopes. Moreover, just in front of the dune crest, the flow velocity is highest for slope inclinations of 50° and 60° (Figure 15A).
Figure 15B shows the cross-shore flow velocities on the dune top. The results show that the steeper the dune slope, the stronger the decrease in flow velocity at the dune crest. Physically, this can be explained by the fact that a larger change in slope causes a pressure drop close to the surface: Most of the flow 'wants' to keep momentum and not stay attached to the surface. Moreover, the flow velocity on the dune

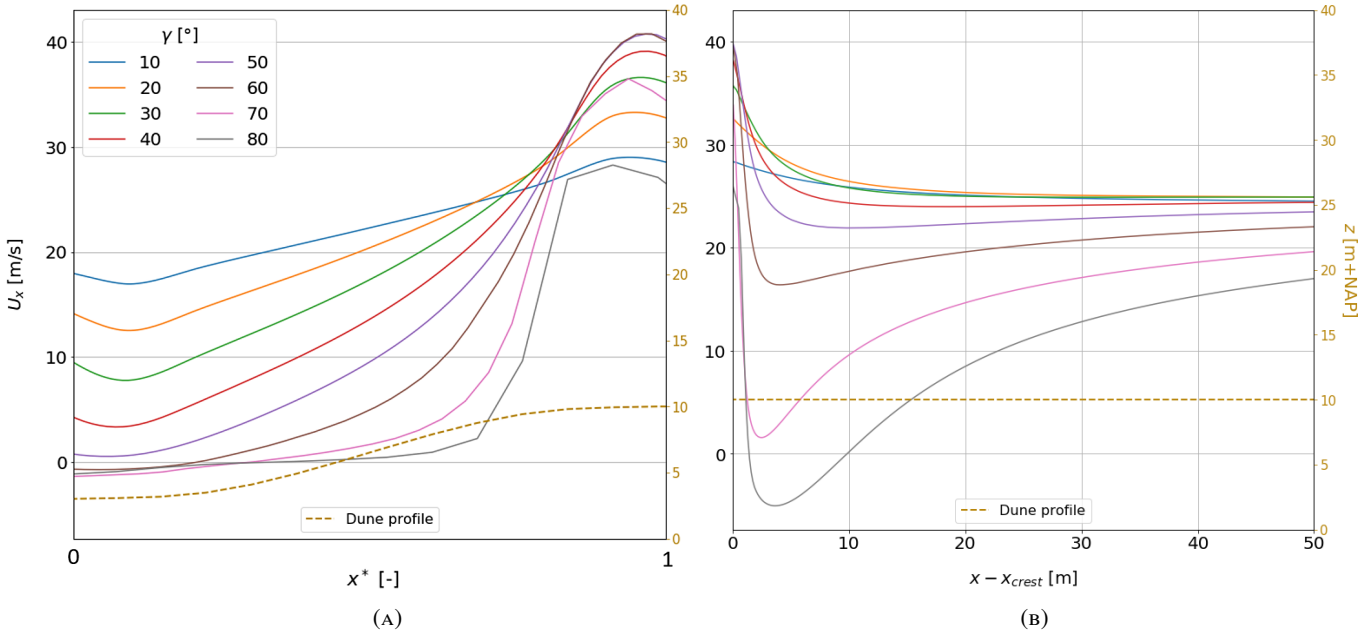


(A) (B)

FIGURE 15: Cross-shore flow velocity ($U_x$, 25 cm above the surface) for an incident wind angle of 0° and different dune slope inclinations (solid line colors). (A) Dune slope. (B) Dune top.

top reaches negative values for a slope inclination of 80°, meaning that flow reversal and flow separation occur (Figure 15B, see also Figure 14B).

Figure 16 shows the change in flow direction for an incident wind angle of 15° and different slope inclinations. Again, the cross-shore dune slope width is normalized to account for the changes in length due to changes in slope inclination.

First of all, the figure shows that at the dune toe, the location with the highest flow direction angle is moving towards the beach with an increasing dune slope inclination (Figure 16A, Figure 16B). In addition, at the dune toe, the jump in flow direction angle between a slope of 40° and 50° is much larger than the other changes. On the other hand, on the dune top, the flow direction is largely the same for slope inclinations of 10°-60° (close to 15°), while 70° and 80° slope inclinations give very different results

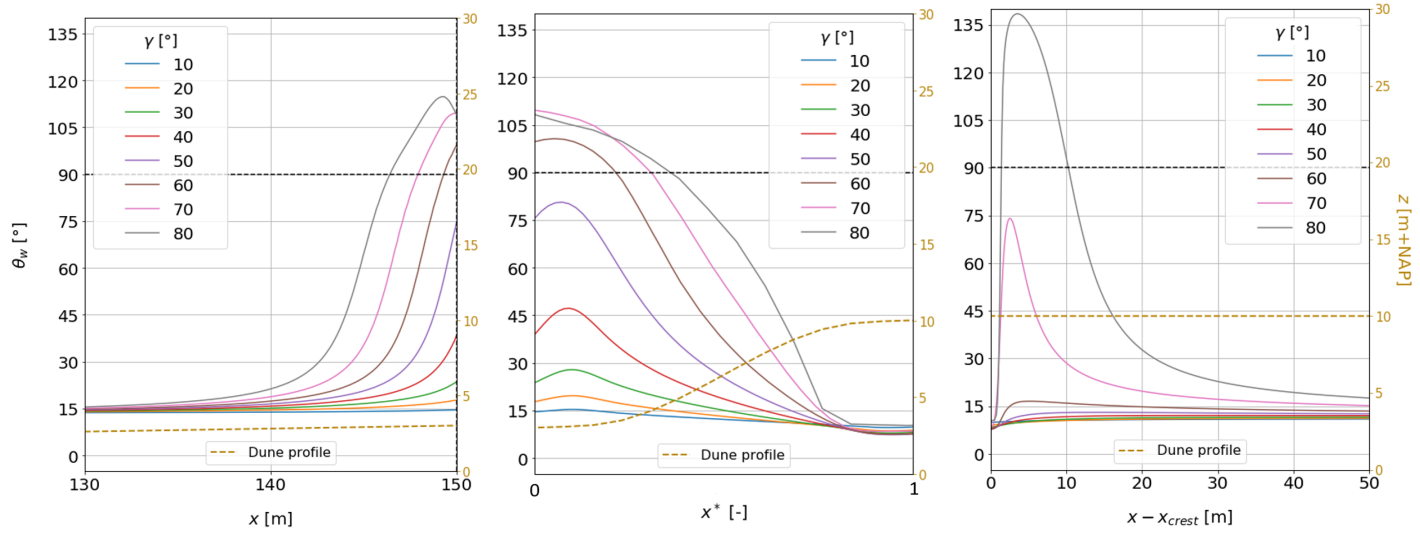


(A) (B) (C)

FIGURE 16: Change in flow direction ($\theta_w$, 25 cm above the surface) for an incident wind angle of 15° and different dune slope inclinations (solid line colors). (A) Beach until dune toe. (B) Dune slope. (C) Dune top.

(Figure 16C). Moreover, the figure shows that flow reversal occurs at the dune toe for slopes higher than approximately 55° (Figure 16B). Lastly, the flow deflects increasingly longshore, until flow reversal starts to occur at 80° (Figure 16C).

### 4.1.3 Combined impact on flow patterns

Lastly, the combined impact of incident wind angle and dune slope on the flow patterns around the dune is visualized. Varying both the incident wind angle and the dune slope gives different flow velocity values over the whole domain. Therefore, the flow velocity variation is shown at two specific locations (Figure 17): at the dune toe and at 3 m landward of the dune slope (locations 1 and 3, Figure 18). The latter location was chosen to gain more insight in the interesting dynamics that occur landward of the dune crest, especially for steeper slopes (Figure 14B, Figure 15B).

Figure 17A shows that the flow velocity magnitude at the dune toe decreases for steeper slopes and lower incident wind angles. Moreover, it shows that the impact of wind direction on the flow velocity is much greater at steeper slopes. In addition, Figure 17B shows that the cross-shore flow velocity at the dune toe decreases for steeper slopes. Furthermore, for most slope inclinations (10°-50°), the cross-shore

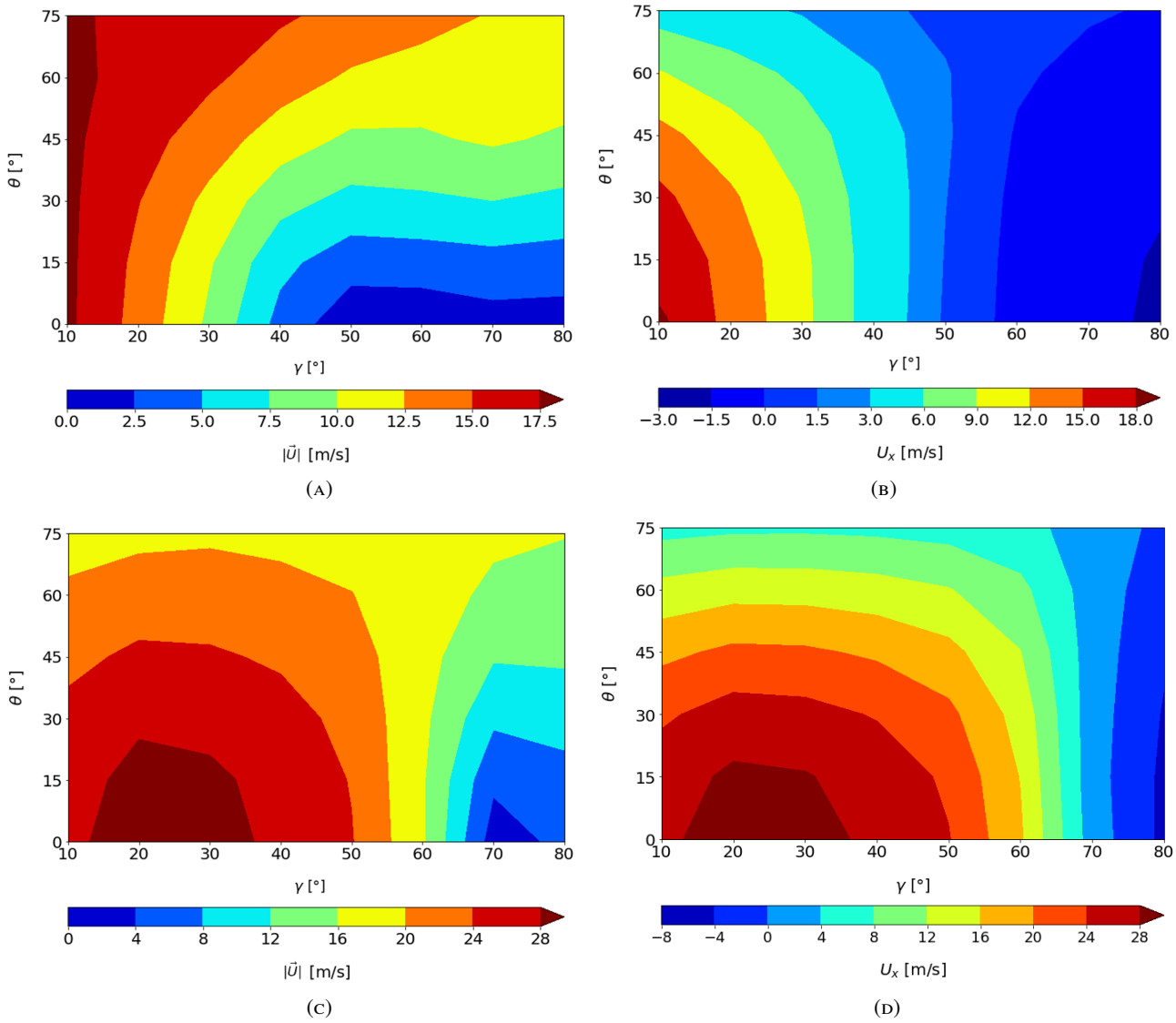


FIGURE 17: Flow velocity variation at the dune toe and on the dune top (locations 1 and 3, Figure 18) for all dune slope inclinations ($\gamma$) and incident wind angles ($\theta$). (A,B) Flow velocity magnitude ($|\vec{U}|$) and cross-shore flow velocity ($U_x$) at the dune toe. (C,D) Flow velocity magnitude ($|\vec{U}|$) and cross-shore flow velocity ($U_x$) on the dune top.

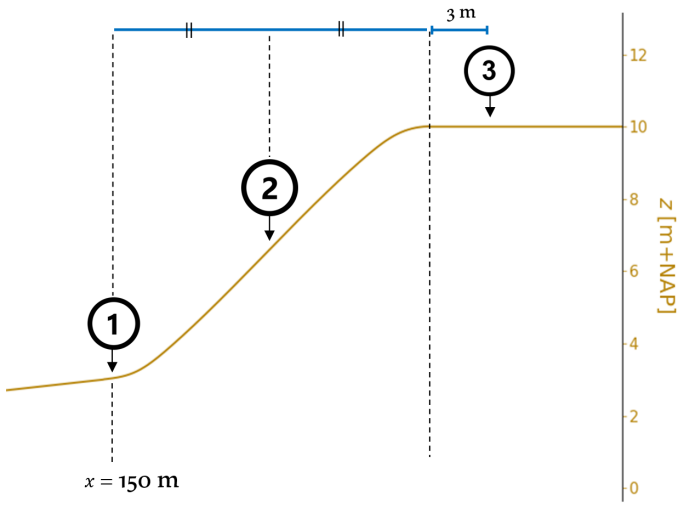


FIGURE 18: Locations used in visualization of air flow and sediment transport patterns. **(1)** Dune toe ($x = x_{toe} = 150$ m). **(2)** Halfway on the dune slope $\left(x = (x_{toe} + x_{crest})/2 \text{ m}\right)$. **(3)** 3 m landward of the dune crest ($x = x_{crest} + 3$ m).

flow velocity increases for lower incident wind angles. For steeper slopes, however, it decreases for lower incident wind angles, albeit to a lesser extent.
On the dune top, 3 m landward of the dune crest, the flow velocity varies in relation to the incident wind angle and dune slope inclination in multiple ways (Figure 17C, Figure 17D). For most slope inclinations (10°-50°), the flow velocity magnitude increases for lower incident wind angles. For the steepest slopes (70° and 80°), however, it decreases for lower incident wind angles, albeit to a lesser extent (Figure 17C). Moreover, the largest flow velocities, both in magnitude and cross-shore direction, are present for small incident wind angles (0°-15°) and relatively small dune slope inclinations (20°-30°).

Finally, Figure 17B and Figure 17D show two other interesting results. First, by comparing the figures to the flow velocity magnitude at the corresponding locations, it shows that for $\theta > 0$, $|\vec{U}| \neq 0$ where $U_x = 0$. Therefore, the parameters for which there is only longshore (and possibly vertical) flow present are found. Secondly, the set of conditions for flow reversal at the dune toe and on the dune top are shown, in the region where negative cross-shore flow velocities occur. At the dune toe, this occurs for slope inclinations of 60°-80° for low incident wind angles, and only for a slope inclination of 80° for high incident wind angles. On the dune top, flow reversal occurs only for slope inclinations greater than 70°.

## 4.2 Aeolian sediment transport

From the results of the previous sections, it is expected to see a significant impact of both the incident wind angle and the dune slope on the sediment transport. The sediment transport is calculated using the methods discussed in the previous chapter (section 3.3.1). This will be explored below. First, the influence of the incident wind angle will be discussed. Secondly, the influence of the dune slope will be investigated. Finally, the combined impact of the incident wind angle and the dune slope will be discussed.

### 4.2.1 Impact of incident wind angle on sediment transport

The change in sediment transport magnitude for variations in incident wind angle and a 20° dune slope is shown in Figure 19. The general pattern is mostly the same as the flow velocity pattern (Figure 13): there is a decrease at the dune toe, a strong increase over the dune slope and a decrease towards a base value on the dune top. Again, the base value increases for more shore-normal wind directions (further exploration in section 4.4.2). However, there are also a few differences. First of all, on the dune slope, a much stronger increase is seen, which is explained by the cubic relationship between the shear velocity and sediment transport. Moreover, on the dune top, just landward of the dune crest, there is another increase after the

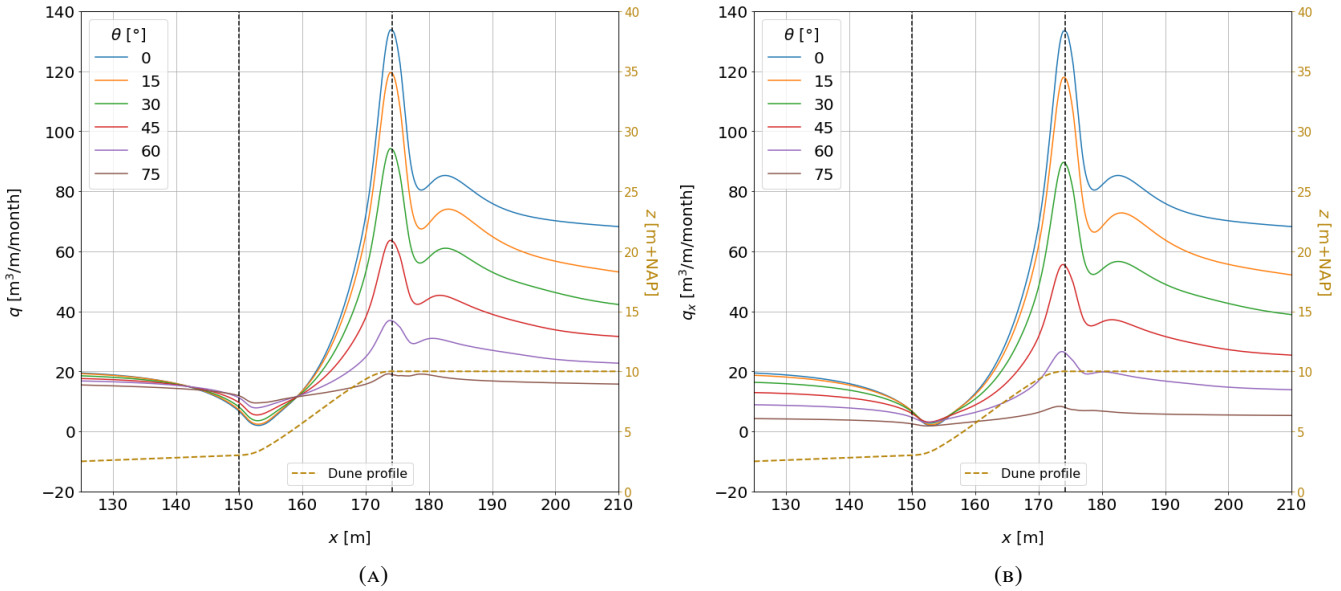


FIGURE 19: Change in sediment transport for a dune slope inclination of 20° and different incident wind angles (solid line colors). (A) Transport magnitude ($q$). (B) Cross-shore transport ($q_x$).

initial decrease, which is not present in the flow velocity. This 'bump' moves towards the dune crest and dampens out for higher incident wind angles. Furthermore, the peak sediment transport is reached exactly on the dune crest ($x = x_{crest}$), whereas the peak flow velocity moved seaward for lower incident wind angles. The second and third difference show that the shear stress (and therefore the shear velocity) on the surface does not entirely follow the same pattern as the flow velocity at 25 cm above the surface.

Although the incident wind angle clearly impacts both the sediment transport magnitude and the cross-shore sediment transport, comparing Figure 19B to Figure 19A shows that the impact on the cross-shore sediment transport is noticeably larger. On the beach, there is an increase of approximately 400% from the highest to the lowest incident wind angle. Furthermore, over the dune slope, this grows to an increase of approximately 1500% at the dune crest. This shows how impactful the orientation of the dune relative to the incident wind angle is in terms of sediment transport towards the dune and in the dune.

### 4.2.2 Impact of dune slope on sediment transport

Figure 20 shows the change in sediment transport over the dune slope for variations in dune slope and a 60° incident wind angle. Note that the sediment transport is plotted in a log scale, because of the large differences in sediment transport values. The pattern is quite similar to the flow velocity pattern on the dune slope (Figure 15A): there is a decrease in sediment transport at the dune toe for steeper slopes, and an increase over the dune slope. However, around the dune crest ($x^* = 0.9$–$1$), the sediment transport magnitude increases steadily with an increase in dune slope inclination (Figure 20A). This pattern is not present in the flow velocity at 25 cm above the surface. Also, the minimum at the dune toe and the peak in sediment transport at the crest move seaward with steeper slopes. This effect is strongly visible for the sediment transport, whereas this did not show up in the results of the flow velocity.

The cross-shore sediment transport shows mostly the same patterns as the sediment transport magnitude (Figure 20B). However, the pattern seems to be squeezed towards the landward side of the slope. For steeper slopes, it takes longer for the cross-shore sediment transport to 'catch up' than for the sediment transport magnitude. Furthermore, the figure shows that most of the sediment is transported longshore, which is expected for an incident wind angle of 60°. Despite this expectation, it is still interesting to see that for a dune slope inclination of 40° or higher, there is almost no sediment transport in cross-shore direction. This means that hardly any sand from the beach would reach the dunes and is transported longshore or deposited upwind of the dune toe.

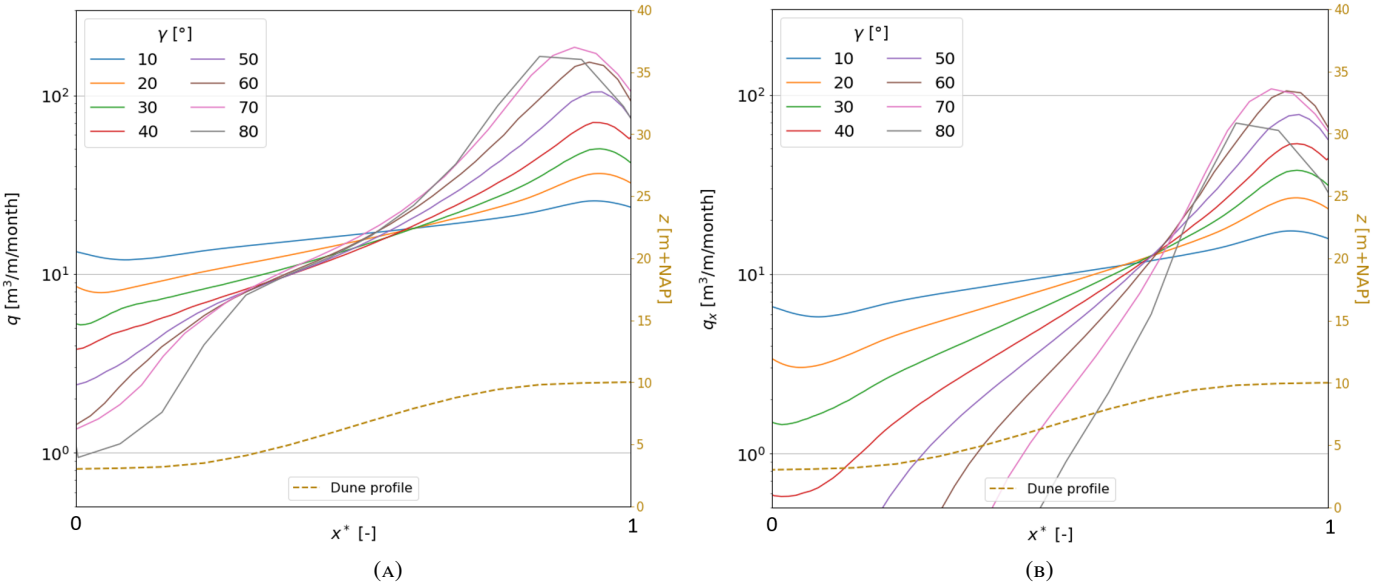


FIGURE 20: Change in sediment transport over the dune slope for an incident wind angle of 60° and different dune slope inclinations (solid line colors). (A) Transport magnitude ($q$). (B) Cross-shore transport ($q_x$).

### 4.2.3 Combined impact on sediment transport

The combined impact of incident wind angle and dune slope on the sediment transport in the dune is visualized. Varying both the incident wind angle and the dune slope gives different sediment transport values over the whole domain. Therefore, the sediment transport variation is shown at three specific locations: at the dune toe, halfway on the dune slope, and 3 m landward of the dune slope (locations 1, 2, and 3, Figure 18). Both cross-shore and longshore sediment transport patterns are investigated at these locations.

The variation in cross-shore sediment transport for the three locations is shown in the left column of Figure 21. Figure 21A, where the sediment transport at the dune toe is depicted, portrays only a small region with negative (seaward) sediment transport. This can be explained by the combination of a reasonably strong flow velocity and a negative (seaward) cross-shore velocity which occurs in that region (Figure 17A, Figure 17B). So while there is a reasonably large set of parameters leading to flow reversal at the dune toe (Figure 17), the seaward sediment transport at the dune toe is very small, since there are no large seaward velocity components.

Furthermore, the cross-shore sediment transport halfway on the dune slope exhibits a clear pattern (Figure 21C): At this location, the cross-shore sediment transport increases both with a decrease in slope and a decrease in incident wind angle. The former effect is expected from the fact that lower incident wind angles naturally result in a stronger flow in the cross-shore direction. The latter effect can be explained by what is seen from Figure 15A and Figure 20B: for steeper slopes, it takes longer for the flow to speed up and therefore, the cross-shore sediment transport is lower halfway on the slope.

In Figure 21E, the cross-shore sediment transport 3 m landward of the dune crest is shown. This figure shows that the cross-shore sediment transport can be both strongly seaward and strongly landward, depending on the incident wind angle and dune slope. Additionally, it shows that negative (seaward) transport starts to occur on top of the dune for slopes of 70° and higher. This is different from the cross-shore flow velocity at 25 cm above the surface, where flow reversal on the dune top only occurs at slopes steeper than 70° (Figure 17D). Although this set of parameters for seaward transport is smaller than at the dune toe, much more significant magnitudes are reached here. This can be explained by the much stronger seaward flow velocities that occur here (Figure 17D). Also, a maximum landward sediment transport is seen at this location for a slope inclination of 40° and an incident wind angle of 0°, which is different from the location of strongest flow velocity (Figure 17C, Figure 17D).

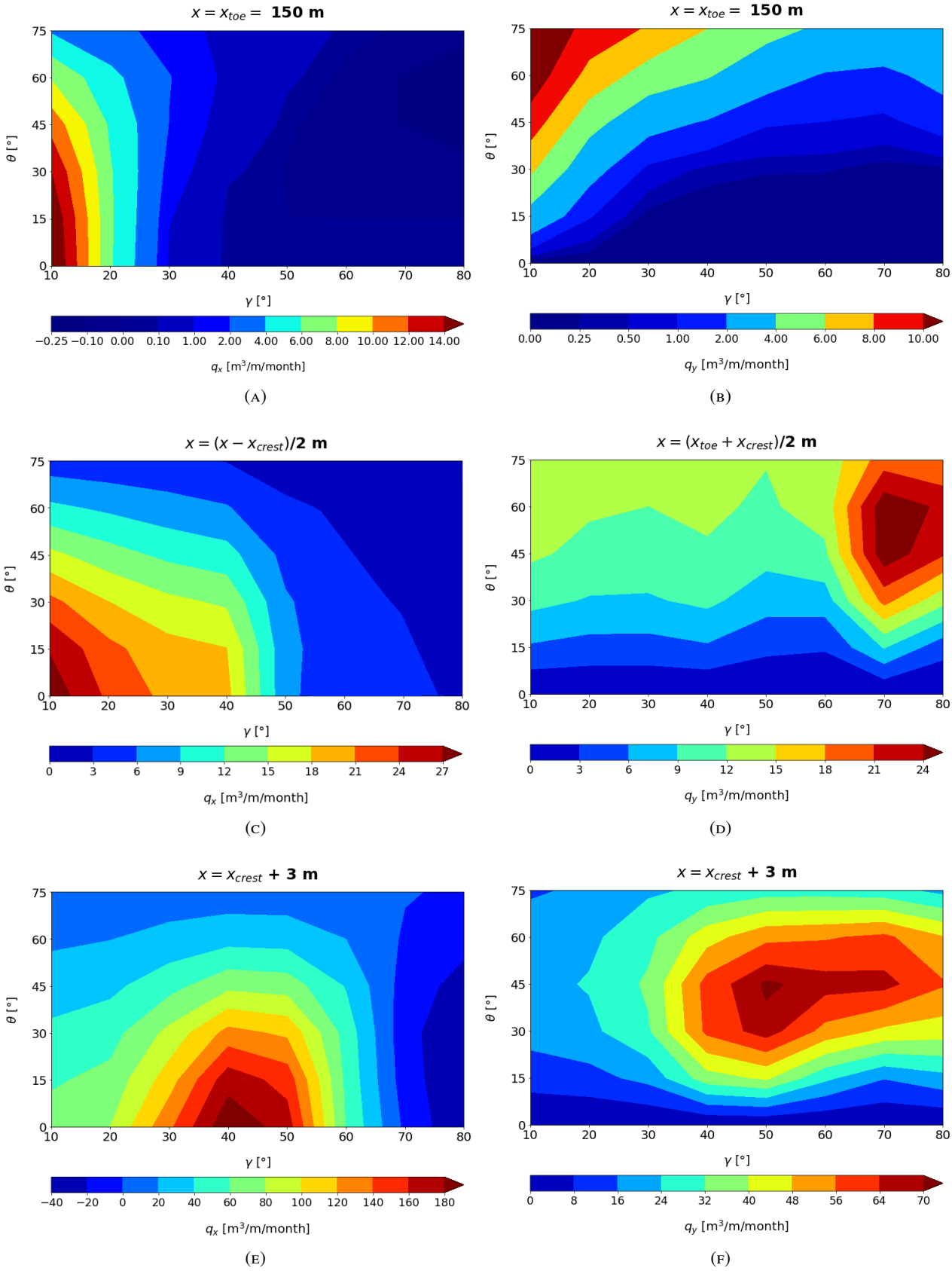


FIGURE 21: Cross- and longshore sediment transport ($q_x$ and $q_y$) variation at the dune toe, halfway on the dune slope, and on the dune top (locations 1, 2, and 3, Figure 18) for all dune slope inclinations ($\gamma$) and incident wind angles ($\theta$). (A, C, E) $q_x$ at locations 1, 2, and 3, respectively. (B, D, F) $q_y$ at locations 1, 2, and 3, respectively.

The variation in longshore sediment transport for the three locations is shown in the right column of Figure 21. The longshore sediment transport at the dune toe depicts a clear pattern (Figure 21B): At this location, the longshore sediment transport increases both with a decrease in slope and an increase in incident wind angle. These are expected effects from the fact that higher incident wind angles result in a stronger flow in the longshore direction and steeper slopes result in a lower flow velocity at the dune toe (Figure 17A).

Moreover, Figure 21D, where the sediment transport halfway on the dune slope is depicted, shows that for lower incident wind angles (up to 30°), the longshore sediment transport is mostly independent of the dune slope inclination. In addition, a clear increase in transport is shown with an increase in incident wind angle, although this general pattern stops at 60°, since a maximum seems to be reached for a slope inclination of 70° at an incident wind angle of 45-60°.

Lastly, Figure 21F shows the longshore sediment transport 3 m landward of the dune slope (on top of the dune). This figure shows that the longshore sediment transport at this location is strongest for incident wind angles of 45° for all slope inclinations. It is interesting to see that higher incident wind angles than 45° do not lead to more longshore sediment transport at this location. The maximum is reached for a slope inclination of 50°.

## 4.3 Morphological change

In this section, the morphological change resulting from the sediment transport is investigated. Using Equation 11 (section 3.3.2), the sedimentation and erosion can be predicted throughout the domain. First, the morphological change over multiple time scales is shown. Secondly, the impact of the incident wind angle is investigated. Following that, the sedimentation at the dune toe for all slope inclinations and incident wind angles is investigated. Lastly, a simple implementation of the influence of vegetation is used to show the effect of vegetation on the sediment transport and morphological change on the dune profile.

### 4.3.1 Morphological change over multiple time scales

Using a time step of 1 day, 1 week and 1 month, an incident wind angle of 60° and a dune slope inclination of 20°, Figure 22 is generated. A time step of 1 month is chosen, to clearly show the morphological change pattern that occurs over the domain. Similarly, the morphological changes for a time step of a day and a week have the same pattern, only scaled by a factor. The figure shows the cross-shore sediment transport over the domain, the initial dune profile, and the updated dune profiles.

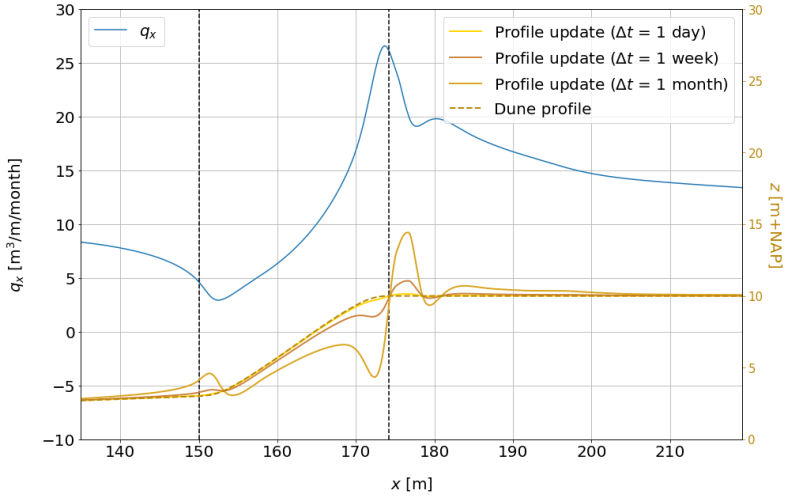


FIGURE 22: Sediment transport with a day, a week and a month of sedimentation and erosion over the domain for an incident wind angle of 60° and a dune slope inclination of 20°.

A few results are highlighted from this figure. First, sedimentation is shown in front of and on the dune toe, where the updated profile after a month is approximately 1.5 m higher than the original profile. In addition, on the dune slope, very strong erosion is present. This comes from the strong increase in flow velocity and therefore sediment transport over the dune slope. Relating this to dunes in the field, it shows the importance of vegetation on the dune slope, especially near the dune crest. Lastly, on the dune top, more sedimentation and erosion is found. A portion of the sediment that was picked up on the dune slope is deposited on the dune crest, due to the decrease in flow velocity and therefore sediment transport at the crest. The rest of the sediment is spread out over the dune top.

### 4.3.2 Impact of incident wind angle to morphological change in storms

Since a month of having wind speeds of 20 m/s is quite unrealistic, the morphological changes due to a storm of two days are investigated. Figure 23 shows the morphological change ($\frac{\partial z_b}{\partial t}$) over the domain for a time step of two days for a dune slope inclination of 20° and different incident wind angles. Clearly, the impact of incident wind angle can be seen, showing almost no sedimentation and erosion for a storm with a wind angle of 75°, while a storm incoming at 0° shows a few meters of erosion on the dune slope and deposition on the dune top.

Moreover, the figure shows that the impact on the morphological change of a small difference in incident wind angle varies. For instance, the difference in sedimentation and erosion for the change in wind angle from 0° to 15° is much smaller than a change from 30° to 45°.

Finally, no matter what the incident wind angle, erosion starts to occur at the same point on the dune slope. This location is called $x_{ero}$ and is estimated at $x_{ero} = x_{toe} + DW/6$.

### 4.3.3 Sedimentation variation at the dune toe

The sedimentation variation in the area around the dune toe, is shown in Figure 24. This shows the net cross-shore sediment transport in m$^3$/m/month (second method in section 3.3.2, $q_x\big|_{x=140} - q_x\big|_{x=x_{ero}}$). The second location ($x_{ero}$) was chosen to estimate the sedimentation around the dune toe, without taking into account the erosion that occurs on the dune slope. Again, it is seen that low incident wind angles lead to more sedimentation, regardless of dune slope inclination. This is caused by the stronger decrease in cross-shore flow velocity and thus in cross-shore sediment transport. An interesting result is that the strongest sedimentation at the dune toe occurs for a dune slope inclination of 20°.

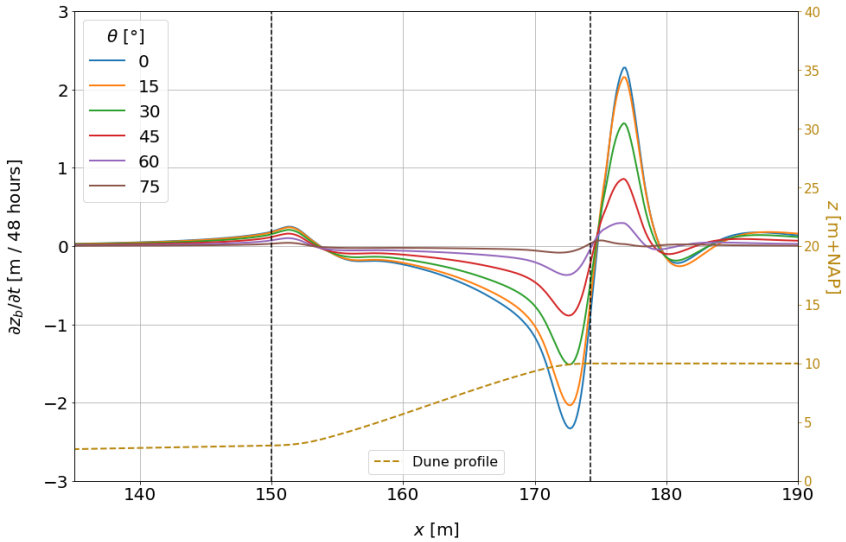


FIGURE 23: Sedimentation and erosion over 48 hours for a dune slope inclination of 20° and different incident wind angles (solid line colors).

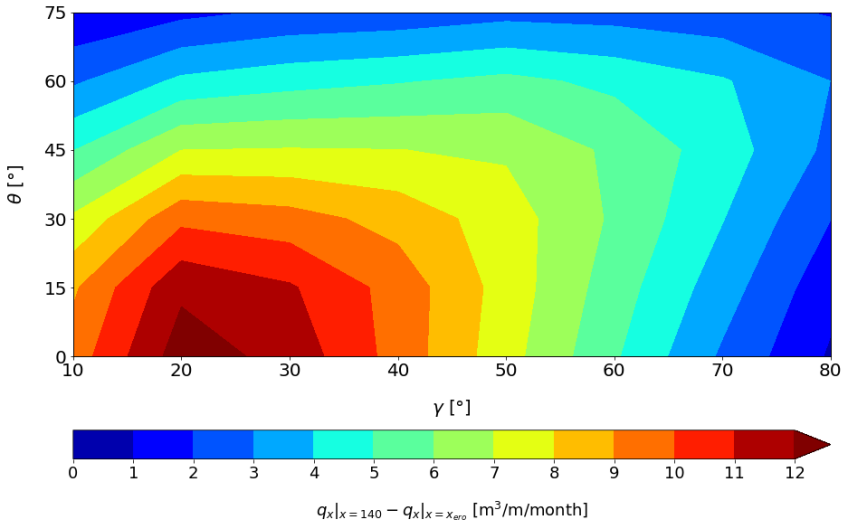


FIGURE 24: Variation in accumulation of sediment around the dune toe $\left(q_x\big|_{x=140} - q_x\big|_{x=x_{ero}}\right)$.

### 4.3.4 The effect of vegetation on sedimentation

Since the erosion on the dune slope is large and it is well-known that dune vegetation stabilizes a dune and counteracts erosion, a simple implementation of vegetation on the dune slope and dune top is investigated. A method for the implementation of vegetation in a model was proposed by Durán and Moore (2013), which was used by Roelvink and Costas (2019) for calculating sediment transport in coastal dunes. This method uses an adaptation to the shear velocity at a location to simulate vegetation. In the same way as the study by Roelvink and Costas (2019), and assuming a somewhat conservative effectiveness of the vegetation in slowing down the air flow to simulate not fully grown vegetation, the effect of vegetation is implemented in the following way: for all $x$-values greater than $x_{toe}$, the shear velocity ($u_*$) is divided by a factor 1.5.

Figure 25 shows the cross-shore sediment transport over the domain for an incident wind angle of 60° and 75°, and a dune slope inclination of 20°. Moreover, the initial dune profile and the updated dune profiles are shown to show the changes that occur, using a time step of 1 month.

At the dune toe, the (cross-shore) sediment transport is fully stopped, inducing strong sedimentation at

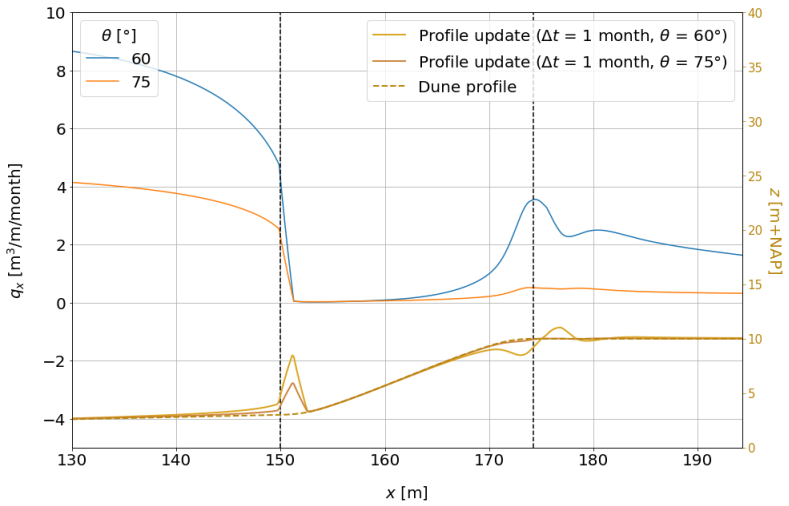


FIGURE 25: Sediment transport with a month of sedimentation and erosion over the domain for an incident wind angle of 60° and 75°, and a dune slope inclination of 20°. The influence of vegetation is included to simulate what happens when the dune slope and dune top are covered in vegetation.

that location. Comparing this result to Figure 20B shows the impact of the 'vegetation' implementation, where cross-shore sediment transport is clearly present for an incident wind angle of 60° and a slope inclination of 20°. Still some erosion just upwind of the dune crest occurs, which is again deposited just downwind of the dune crest, but much less than before (Figure 22). Moreover, the difference in sedimentation and erosion between an incident wind angle of 60° and 75° is much larger around the dune crest than at the dune toe.

Lastly, Figure 26 shows the variation in accumulation of sediment around the dune toe, with the inclusion of the influence of vegetation on the shear velocity. Note that the scale is different from Figure 24. A closer examination of the two figures shows an interesting result: the sedimentation values for slopes steeper than 50° do not vary from the 'unvegetated' situation, yet for slope inclinations less than 50°, there is a clear increase in sedimentation at the dune toe. This can be explained by the fact that steeper slopes already have little to no cross-shore shore sediment transport at the dune toe without vegetation (Figure 20B, Figure 21A). The 'vegetation' implementation causes the (cross-shore) sediment transport of the less steep slopes to strongly decrease at the dune toe, causing sedimentation there. In addition, a notable observation is the fact that the impact of the incident wind angle on the sedimentation at the dune toe varies. In particular, the difference in sedimentation for a small change in low wind angles is much less impactful than a small change in high wind angles (except for very steep slopes). For example, with a slope inclination of 10°, the change from $\theta = 15°$ to $\theta = 30°$ (16 $m^3$/m/month to 14 $m^3$/m/month) is much less impactful than the change from $\theta = 60°$ to $\theta = 75°$ (8 $m^3$/m/month to 4 $m^3$/m/month): not only because the latter difference is larger, but even more because the proportional change is much larger.

## 4.4 Model sensitivity

In this section, the differences in simulation results will be shown for the following cases:

- $k$–$\epsilon$ opposed to the RNG $k$–$\epsilon$ turbulence closure model
- Domain height of 50 m opposed to a domain height of 100 m
- Bed roughness length of 0.0001 m opposed to 0.0003 m

Comparisons are made by varying the wind angle between 15°, 45° and 75°, with a constant dune slope of 30°.

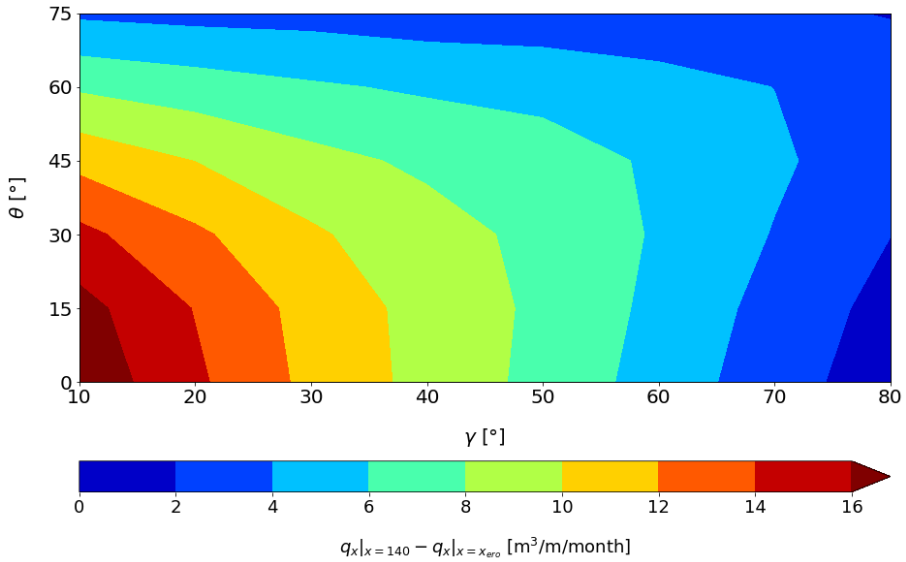


FIGURE 26: Variation in accumulation of sediment around the dune toe $\left(q_x\big|_{x=140} - q_x\big|_{x=x_{ero}}\right)$. The influence of vegetation is included to simulate what happens when the dune slope and dune top are covered in vegetation.

### 4.4.1 Turbulence models

The research by Smith et al. (2017a) has shown differences in simulation results between the $k$–$\epsilon$ and the RNG $k$–$\epsilon$ turbulence closure model, and they concluded that in the case of barchan dunes, the RNG $k$–$\epsilon$ model is more accurate in simulating the flow. Therefore, it is relevant to check the differences within the scope of this research.
The flow velocity differences are shown in Figure 27. Approximately the same flow patterns are found. However, the decrease of flow velocity at the dune toe and on the dune top is stronger with the RNG $k$–$\epsilon$ model, leading to a difference of about 1-2 m/s at those locations.

However, the bed shear stress shows very different behavior. Clearly, over the whole domain, the bed shear stress is lower in magnitude when the RNG $k$–$\epsilon$ model is used. However, the biggest change occurs just downwind of the dune crest, where the decrease in bed shear stress and the increase thereafter are much larger. This would lead to a significant change in sedimentation on the dune crest: much more sediment would be deposited close to the dune crest. Additionally, downwind of this deposition, the erosion would be much stronger as well.

### 4.4.2 Domain height variation

The maximum vertical value over the domain and the inlet height used in the simulations is equal to 50 m, under which the surface increases over the beach and the dune. However, continuity dictates that the flow volume coming in at the inlet should exit at the outlet. This means that a fictional flow speed-up is expected in $x$-direction on the top of the dune, since the domain height is lower at the outlet than at the inlet. Indeed, some speed-up over the dune top was seen in the simulation results (e.g. Figure 13). Due to volume continuity and the fact that the top of the domain is seen as a closed boundary (`slip`), all flow coming in at the domain inlet, should exit at the domain outlet. Since a 10 m dune height was used, it is expected that the cross-shore flow velocity ($U_x$) will approximately speed up by a factor of $50/40 = 1.25$. Therefore, there is clearly less speed-up visible on top of the dune with a domain height of 100 m instead of 50 m (Figure 28A). However, the effect is still there and is not negligible. Also, the bed shear stress (Figure 28B) clearly shows a decrease in magnitude on the dune top.

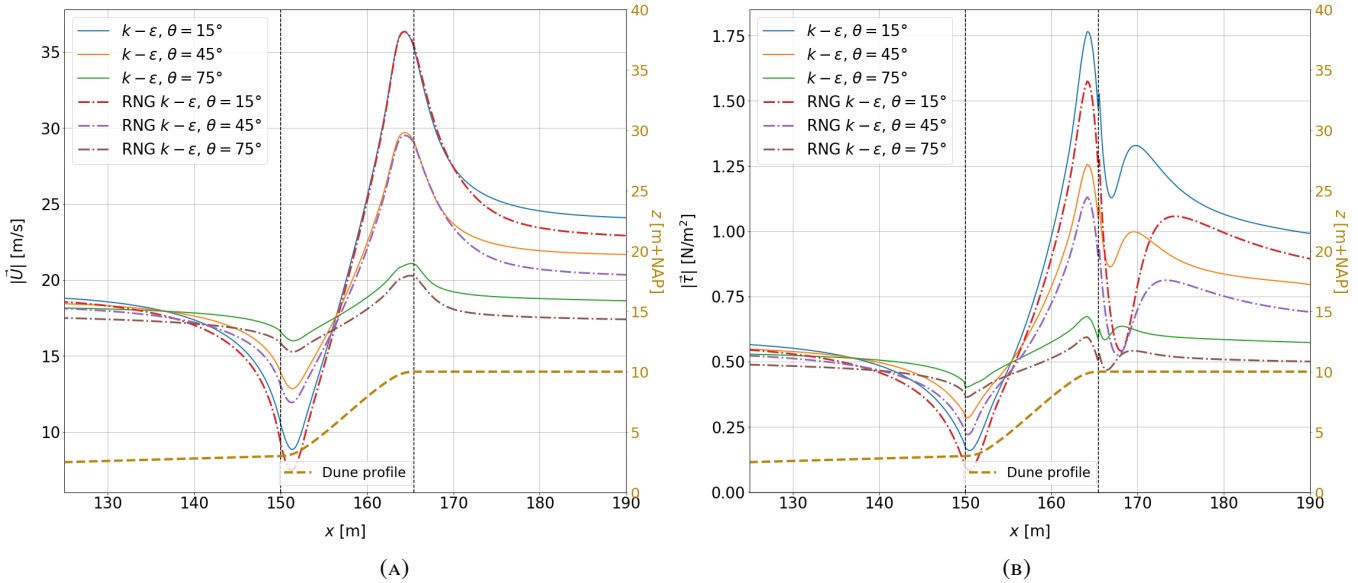


(A) (B)

FIGURE 27: Flow velocity ($|\vec{U}|$, 25 cm above the surface) and bed shear stress ($|\vec{\tau}|$) magnitude for a dune slope of 30° and varying wind directions (line colors) for different turbulence closure models. The models used are the $k$–$\epsilon$ and the RNG $k$–$\epsilon$ model. (A) Flow velocity. (B) Bed shear stress.

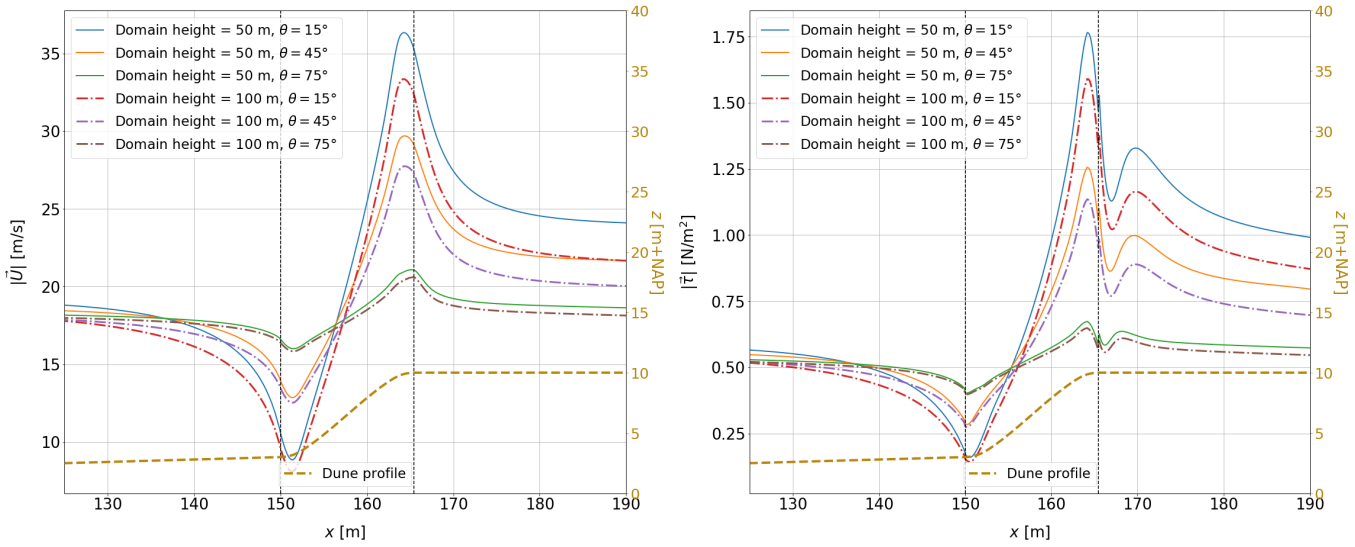


(A) (B)

FIGURE 28: Flow velocity ($|\vec{U}|$, 25 cm above the surface) and bed shear stress ($|\vec{\tau}|$) magnitude for a dune slope of 30° and varying wind directions (line colors) for different domain heights. The domain heights used are 50 and 100 m. (A) Flow velocity. (B) Bed shear stress.

### 4.4.3 Bed roughness

As a final step, a change was made in the bed roughness length, adapting it from 0.0001 to 0.0003. The flow pattern and flow velocities remain roughly the same for an increase in bed roughness length, with only a slight decrease in flow velocity over the profile (Figure 29A). However, an increase in bed shear stress on the beach, from 0.5 to 0.6 N/m$^2$, and an even greater increase on the dune crest are clearly visible (Figure 29B). Since sediment transport is most often scaled with $u_*^2$ or $u_*^3$, and $u_*$ scales with $|\vec{\tau}|^{0.5}$, a notable increase in sediment transport is expected with an increase in bed roughness length.

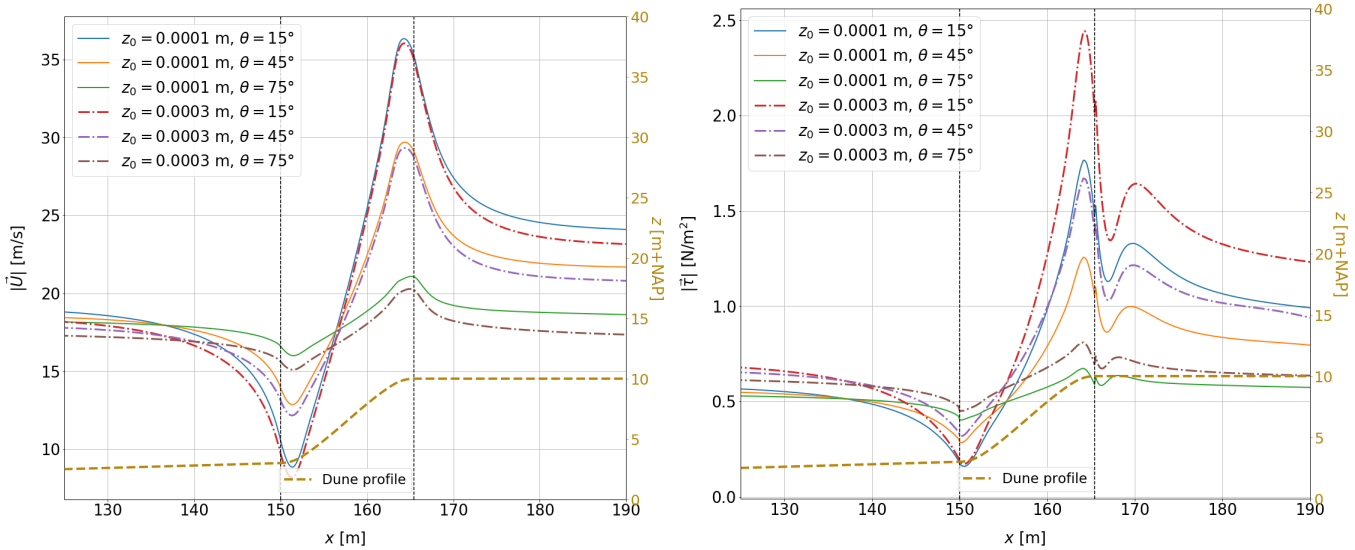


(A) (B)

FIGURE 29: Flow velocity ($|\vec{U}|$, 25 cm above the surface) and bed shear stress ($|\vec{\tau}|$) magnitude for a dune slope of 30° and varying wind directions (line colors) for different bed roughness lengths. The bed roughness lengths ($z_0$) used are 0.0001 m and 0.0003 m. (A) Flow velocity. (B) Bed shear stress.

# 5 Discussion

Many findings are presented in the report, related to air flow and sediment transport patterns over a beach-dune profile. In this chapter, the results and the limitations of this research are discussed.

## 5.1 Interpretation of results

The research results on flow and sediment transport patterns are discussed and interpreted in this section. Also, a comparison to data from the Hondsbossche Dunes is done.

### 5.1.1 Flow patterns

The research is in line with flow patterns around dunes found by other researchers, both for the influence of incident wind angle (e.g. Hesp et al., 2015; Tsoar, 1983; Walker et al., 2009b) and dune slope inclination (e.g. Hesp and Smyth, 2021; Tsoar et al., 1996). This validates the use of the model and shows that the model is reliable. Results previously shown by researchers include the following:

- Longshore deflection at the dune toe and stronger cross-shore deflection over the dune slope.
- Return towards initial flow direction at the dune top.
- Strongest flow deflection for incident wind angles of 30°-60°.
- Steeper slopes lead to more deceleration at the dune toe.

However, some additional findings are added by systematic investigation of the influence of incident wind angle and dune slope. First of all, the current research includes an extension to existing research by investigating the combination of the two effects, which lead to more discoveries. It shows that in most cases, the influence of the wind angle depends on what dune slope inclination is present, and vice versa. Moreover, instead of using sharp-edged dunes and scarps, as was done in previous CFD studies, more natural-shaped dunes with rounded edges were used. Furthermore, the impact on the simulation results by making this change is shown as well (Appendix A.2). An interesting difference that is found is that for sharp-angled 'dunes', the lowest and the peak velocity are always at the dune toe and dune top, respectively (e.g. Hesp and Smyth, 2021; Hesp et al., 2015). However, for the more natural dunes, we see a change in location of the lowest and peak velocity over the curved parts, depending on dune slope. In addition, it was found that for a fixed dune slope, the location of the peak velocity moves towards the dune crest with higher incident wind angles, whereas the location of the lowest velocity (at the dune toe) does not change.

Furthermore, the results show that the speed-up over the dune slope does not necessarily increase with increasing steepness ( Figure 15A). This result contradicts the widely-used speed-up formula by P. Jackson and Hunt (1975), that says that steeper slopes induce more speed up at the dune crest. Three possible explanations are the following:

- The flow velocity for the steepest slopes are impacted more by the smoothness of the edge. The stronger change in slope angle could lead to a decrease in flow velocity above the surface, similar to what was found by Davidson et al. (2022).
- A (numerical) mistake occurred in the extraction and/or analysis of the flow velocity. The results also show that the sediment transport does increase for steeper slopes, so the shear velocity does as well.
- The speed-up formula does not work as well for very steep slopes as it does for less steep slopes, which occur more often in nature.

Finally, with the systematic variation in incident wind angle and slope inclination, three flow regimes can be distinguished, based on the results of the near-bed cross-shore flow velocity (25 cm above the surface) at the dune toe and on the dune top (Figure 17): one with no flow separation and reversal, one where it only occurs at the dune toe, and one where it occurs at both the dune toe and on the dune crest. It was found that slopes steeper than approximately $55°$ can lead to flow separation at the dune toe, depending on the incident wind angle ( Figure 17B). This has not been shown before using a CFD model, while it has been measured in the field (Tsoar, 1983). This can be explained by the fact that no other CFD study has done such a systematic investigation into the variation of dune slope inclination. Moreover, it was shown that this result is slightly different when the dune has sharp edges at the dune toe and dune crest (Appendix A.2). In the case of sharp edges, flow separation at the dune toe was found for slope inclinations of $50°$ and higher.

Additionally, flow separation at the dune top is only demonstrated for very steep slopes, starting just above a slope of $70°$ for low incident wind angles (Figure 17D). The difference between sharp- and smooth-edged dunes is even larger here: for sharp-edged dunes, flow separation at the dune top occurs for slopes with an inclination of $40°$ and higher. This shows that sharp edges induce flow separation easier than smooth edges, which is an established phenomenon in the field of fluid dynamics.

A schematic overview of these findings on flow patterns is shown in Figure 30. This figure gives more insight in how different slope inclinations and incident wind angles influence flow separation and reversal. Admittedly, since these results are based on the flow at 25 cm above the surface, some very small separation bubbles could occur for other wind angles and/or slope inclinations, where the flow velocity at this height is positive, but flow reversal occurs below this height. Moreover, the shape of the dune and the turbulence closure model used in the simulation can influence this result.

### 5.1.2 Sediment transport

The variation in cross- and longshore sediment transport for all combinations of incident wind angle and slope inclination is investigated for three different locations: at the dune toe, halfway on the dune slope, and on the dune top (Figure 21). These locations are chosen in such a way that hopefully, the most important dynamics around the dune slope were captured. This might lead to a biased view, for example that a slope inclination of $40°$ and a wind angle of $0°$ produces the most landward sediment transport on

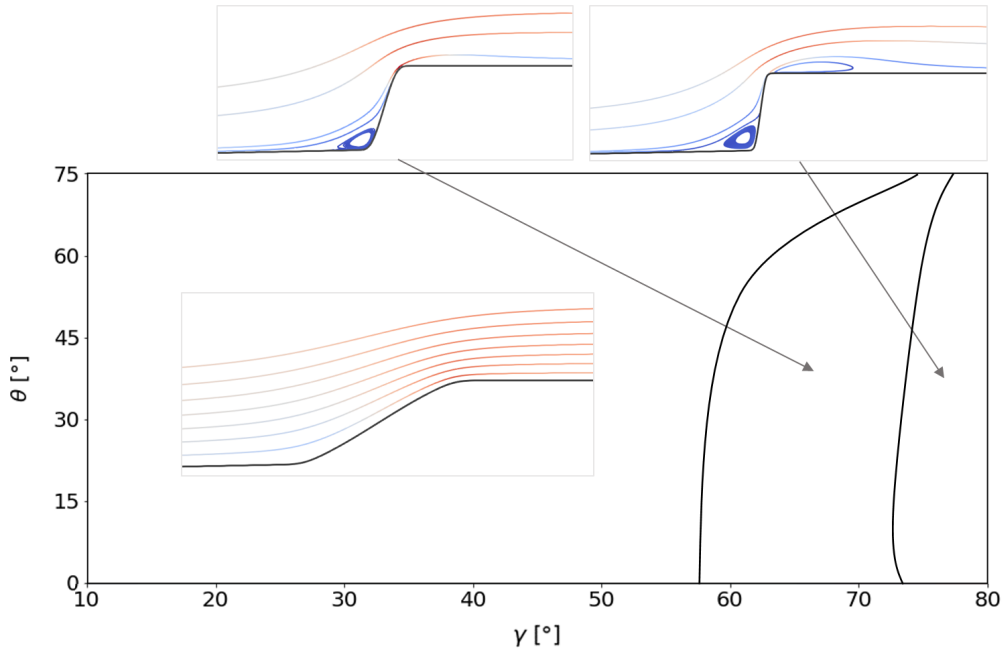


FIGURE 30: Three flow regimes, depending on dune slope inclination and incident wind angle.

top of the dune (Figure 21E). However, this only holds at that specific location.

Similarly, the variation in accumulation of sediment around the dune toe should be carefully observed (Figure 24). The accumulation is portrayed between $x = 140$ m and $x_{ero}$, which is an estimated location on the dune slope where the erosion starts. This might not exactly be the location, since the location varies a little for different slope inclinations. However, it is expected that these changes are very small.

Additionally, it is shown that there is a decrease in sedimentation at the dune toe for steeper slopes (Figure 24), since the sediment coming from the beach will be deposited further away from the slope. This can be explained by Figure 16A and Figure 16B show that the influence of the slope on the wind flow patterns upwind reaches further for steeper slopes. This effect has been shown in previous wind tunnel and field experiments (Qian et al., 2011; Qian et al., 2012).

## 5.2 Limitations

There are still some steps that can be taken to create more reliable predictions for flow patterns and sediment transport in the field. This is due to some assumptions and choices made during this research, which will be discussed in this section. The limitations in model setup, the numerical model, and the sediment transport will be discussed.

### 5.2.1 Model setup

The setup of the computational domain for this research is based on the beach and dune dimensions of the Hondsbossche Dunes. Some choices that have been made are the following:

- The top of the slope is fixed at a height of 10 m. The height of an obstacle in air flow influences the Reynolds number and therefore influences the flow and sediment transport patterns over the domain, although the effect is less for lower slope inclinations (e.g. Hesp and Smyth, 2021; Largeau and Moriniere, 2007). A sensitivity analysis could be done to show the influence of this parameter.
- No longshore variation is present in the model. When present, different flow patterns could be induced.
- A sloping surface is used from the inlet until the dune toe to represent the surface. The slope of this surface (the beach slope) is fixed in the model and was not varied. This might have an influence on the results. This could also be checked using a sensitivity analysis.
- The assumption is made that the beach surface is completely straight. However, this is often not the case, as there are generally foredunes or a flat base/plateau in front of the dune slope. This could also influence sedimentation on the slope, by sediment particles saltating onto the dune slope over the foredune by flow speed-up over the foredune, and/or by the creation of a lee zone behind the foredune where more sediment from the beach is deposited.

Furthermore, the dune shape heavily influences the flow patterns over the domain (Appendix A.2). The smoothed edges of the dune slope were included to make the dune shape more natural, as opposed to previous studies on dune slope variation (e.g. Hesp and Smyth, 2021; Hesp et al., 2015). Although this adaptation does remove the largest gradients in pressure and flow velocity that usually would not occur in natural dune systems, the model still portrays only a schematization of a 'real' dune. For example, the dune investigated in the field study by Davidson et al. (2022) shows a decrease in inclination halfway on the slope, which causes the flow velocity to decrease there because of flow expansion. This phenomenon is not captured in this research and shows how difficult it is to generalize flow patterns and sediment transport patterns for dunes. Also, steep slopes induced by scarping often have a sharp edge at the dune crest, which could lead to different flow and sediment transport patterns. Therefore, more research could be done on the influence of dune shape on the flow patterns around a dune.

### 5.2.2 Numerical model

In this research, assumptions had to be made regarding several settings of the numerical model. As discussed in section 4.4, the simulation results are sensitive to changes in the turbulence closure model, domain height and roughness length. This shows the need for more investigation. More simulations should be done to show how sensitive the results are to changes in the model settings. In this way, for example, an estimate of sediment transport confidence intervals can be calculated for specific situations.

### 5.2.3 Sediment transport

Besides the influence of the numerical model on the sediment transport, there are some other influences that have an effect on the results that are shown in this research.

First of all, moisture content is not included. However, rain and groundwater level can influence the sediment transport strongly.

Moreover, in all dune systems around the world, vegetation plays an important role in the stabilization of the dunes. In this research, most of the results are shown using no vegetation implementation. Only the effect of a simple implementation of vegetation on the sedimentation on the dune was added, to be able to better compare the results to the data from the Hondsbossche Dunes project.

The results without vegetation show very large sediment transport values on the dune slope, which would lead to a quick erosion of the dune. Undoubtedly, a profile such as shown in Figure 22, showing the morphological changes after a month, could not occur in real life. This figure shows what the profile would look like if the instantaneous sedimentation and erosion patterns could continuously occur for a month. However, because the smaller morphological changes in the beginning of the month would lead to changes in the flow patterns, sedimentation and erosion patterns would also change during the month.

Lastly, the sediment transport values shown are based on the empirical formula by Bagnold (1937). Adjustment of the shear velocity threshold for slopes was done using another empirical formula by Iversen and Rasmussen (1994). However, both these equations are not necessarily the best ones and could be replaced by other formulas (e.g. Bagnold, 1973; Kawamura, 1951; Lettau and Lettau, 1978), influencing the results (e.g. Sherman and Li, 2012). Moreover, the transport formula calculates sediment transport without taking into account how high above the surface it is. This could explain the sedimentation found in the Hondsbossche Dunes higher up on the slope. Grains of sand will not only transport over the beach surface and stop right away when the dune slope makes it more difficult for sand to start moving. This means that even when the transport equation implies there is no transport, there could still be some sediment transport in that location.

### 5.2.4 Morphological change simulations

The model could be improved and simulations of morphological change (which make the model more useful in predicting dune evolution) could be done in the following way. First, a simple solution would be to include moisture adjustments for the shear velocity threshold and more precise inclusion of the effect of vegetation. This is a common practice and can produce accurate results (e.g. Van Rijn and Strypsteen, 2020). Subsequently, the sediment transport is much smaller and probably more realistic on the dune slope, leading to less strong erosion and maybe even sedimentation on the dune slope. An even better solution would be to use AeoLiS (section 2.2.3), which includes all mentioned limiting factors for the calculation of sediment transport and sedimentation/erosion patterns. Because AeoLiS has limitations in the calculation of shear velocity at the surface from the wind flow, the shear stresses from OpenFOAM could directly be inserted in the algorithm to improve the results. However, this still does not counteract the fact that the flow patterns change with each change in morphology. Therefore, additionally a morphological loop needs to be created. The best solution would be to create a loop where the following steps are repeated multiple times:

- Run a simulation with OpenFOAM and extract the bed shear stresses
- Load the shear stresses into AeoLiS with the dune profile
- Perform a small number of morphological updates in the time scale of an hour to a day
- Extract the new profile and use it to create a new computational grid

## 5.3 Comparison to the Hondsbossche Dunes

The model domain is based on the dune dimensions of profile type 2 of the Hondsbossche Dunes (section 3.1). Consequently, a comparison of the simulation results can be done with the northern and southern type 2 dune profile, using the measurements of the EcoShape HPZ project.

### 5.3.1 Influence of dune toe orientation

It was found that, on average, sediment transport of 15 $m^3$/m/year into the dune was measured in the first years after construction in the northern part, where the dominant incident wind angle relative to the dune toe equals almost 75° (Figure 6; Bodde et al., 2018). On the other hand, on average 30 $m^3$/m/year of dune sedimentation was measured in the southern part, where the dominant incident wind angle relative to the dune toe equals almost 60° (Figure 6; Bodde et al., 2018). The model results show that the fact that there is twice as much sediment transport into the dune in the southern part can be explained solely by the change in dune toe orientation. Namely, Figure 19B and 25 show that the cross-shore sediment transport over the beach towards the dune is twice as high for an incident wind angle of 60°, compared to an incident wind angle of 75°.

The model results show a transport into the dune ($q_x$ at the dune toe) of approximately 2.5 and 5 $m^3$/m/month, for $\theta = 75°$ and $\theta = 60°$, respectively (for $\gamma = 20°$, see Figure 21A and 25). These values were expected to be larger, as the model assumes a constant wind speed of 20 m/s, which is a very strong wind and does not occur very often (Figure 11). However, even though the values are on the low side, they are in the same order of magnitude to what we would expect. A part of the difference can be explained by the limitations to the model described in the previous section. Moreover, there are other factors that could explain the differences, including the following:

- The wind in the field does not always blow from the same direction, and smaller incident wind angles lead to larger sediment transport towards the dune.
- On a real beach, there are supply-limiting conditions, such as moisture, ripples, and other roughness elements such as shells. This can be partly included in the model by a change in the bed roughness parameter, but to fully capture these elements in a numerical model is difficult.
- The choice of the mean sediment grain diameter ($d$) directly influences the amount of sediment transport. Also, sorting on beaches could lead to changes in sediment grain sizes over time.

### 5.3.2 Sediment deposition pattern

A clear sediment deposition pattern was measured on the dune profile at the Hondsbossche Dunes (Figure 5). Sedimentation at the dune toe is found for both an unvegetated and vegetated dune profile, which is something that is generally observed in dune systems (foredune formation, Figure 22, 23, 24 and 25). However, without the implementation of vegetation, much more erosion and deposition is measured on the dune slope and dune top, respectively, up to 2 m when a storm hits at an incident wind angle of 0° (Figure 23). This amount of erosion and sedimentation, compared to the amount of sedimentation at the dune toe, was not found in the Hondsbossche Dunes. Also, too much landward sediment transport and sedimentation further downwind (on top of the dune) was found (Figure 22). In contrast, the sediment transport and sediment deposition with the vegetation adjustment show results that are much more similar to the data from the Hondsbossche Dunes (compare Figure 7 and 25): much more sedimentation at the

dune toe than on the dune crest, almost no morphological changes on the dune slope, and little to no sediment transport and sedimentation further downwind (on top of the dune). Still, there is some erosion on the dune crest, which was not found in the Hondsbossche Dunes. This could be attributed to the shape of the dune crest, which seems to be too rounded off in comparison to the profile type 2 crestline (compare Figure 7 and 9).

### 5.3.3 Hindcast

With the use of the measured wind directions and wind speed values at the Hondsbossche Dunes, a hindcast could be done of the sediment transport and sedimentation/erosion on the dune profile. For instance, the sum of the different modeled transport values towards the dune can be compared to the total measured accumulation of sand in the dune. Moreover, the sum of the different morphological changes induced by a certain wind speed and incident wind angle could lead to more realistic morphological changes. This can be done without any extra simulations with OpenFOAM, since both the flow velocity and the bed shear stresses scale with the reference wind speed (Appendix A.1). If needed, adaptations to the model, such as different sediment transport equations, sediment grain sizes and bed roughness heights, could be used to calibrate the model to the results found in the Hondsbossche Dunes. In this way, the method presented in this thesis could be validated to provide accurate predictions for sedimentation on a dune profile.

Moreover, using the method described in section 5.2.4, AeoLiS could be used to create predictions with the inclusion of morphological feedback.

# 6 Conclusion and recommendations

In this chapter, the main conclusions and recommendations are discussed.

## 6.1 Conclusion

The aim of the study was to determine the effect of different wind directions (relative to the dune toe) and dune slope inclination on the sediment transport patterns in coastal dunes. This was done in a systematic way, by varying the wind direction from $0°$-$75°$ in steps of $15°$ and the dune slope inclination from $10°$-$80°$ in steps of $10°$. Therefore, in total 48 simulations were done, using an 3D CFD model created with OpenFOAM. With this research, an answer was sought to the question:

> What is the influence of the incident wind angle and slope inclination on the sediment transport patterns in coastal dunes?

First of all, from the simulation results, the near-bed flow velocity patterns (25 cm above the surface) could be analyzed. A new result, found by the use of smooth instead of sharp edges, is that the lowest and peak velocity move over the curved parts, depending on dune slope. Keeping the slope inclination fixed, the location of the peak velocity moves towards the dune crest with higher incident wind angles, whereas the location of the lowest velocity does not change. Moreover, three different flow regimes were found, depending on the incident wind angle and dune slope inclination. The systematic variation of both parameters has provided a better overview of the different flow dynamics that can occur around a dune slope.

Moreover, the bed shear stresses were extracted from the simulation results, to investigate the sediment transport over the beach-dune profile. The results show that the sediment transport pattern at the dune top is different from the near-bed flow velocity. Additionally, steeper slopes lead to more deceleration at the dune toe and therefore a decrease in sediment transport. However, since a threshold value needs to be exceeded before sediment transport occurs, there is no seaward sediment transport for each combination of incident wind angle and dune slope where there is seaward air flow at the dune toe. The systematic changes in incident wind angle and slope inclination show that the sediment transport strongly depends on both parameters. Moreover, by combining the two parameters, it is shown that different sediment transport dynamics can occur, depending on either parameter. The dependency of the sediment transport in both cross- and longshore direction on both parameters is shown for three locations that were investigated in this research: at the dune toe, halfway on the dune slope, and on the dune crest.

Using the Exner equation, some conclusions can also be drawn related to the sedimentation on the dune profile. Sedimentation around the toe of an unvegetated dune slope, caused by the decrease in flow velocity and cross-shore sediment transport, is shown to be largest for a slope inclination of $20°$ and an incident wind angle of $0°$. With this wind angle, large variations in sedimentation are found between different slope inclinations. The sedimentation with more oblique winds, which are more common in the Netherlands, is lower and less sensitive to changes in slope inclination. Additionally, a large amount of erosion on the slope is shown when vegetation is not included in the model, caused by the strong increase in flow velocity and cross-shore sediment transport over the slope. This is especially the case for low incident wind angles, where a storm of 48 hours can lead to up to 2 m of erosion. Importantly, the inclusion of vegetation (by an adaptation to the shear velocity) in the model leads to key differences in the results. The ‘vegetation’ causes a stronger decrease in sediment transport at the dune toe, causing more sedimentation there. In this case, most sedimentation at the dune toe is found for the least steep slopes and the lowest incident wind angles, but no changes are found for slope inclinations of $50°$ and higher.

A comparison of the results with the conclusions drawn from the Hondsbossche Dunes project are promising. First, the influence of the dune toe orientation on the sedimentation on the dune profile is shown to be large. In alignment with the field measurements, the difference found by a change in

orientation of 13° between the northern and southern profile type 2 dune profile can halve the sediment transport into the dune. However, this conclusion cannot be drawn in general. The results show that for smaller incident wind angles and/or steeper slopes, a change of 13° is much less impactful.

Moreover, the inclusion of vegetation in the model provided the possibility for better comparison of the sediment deposition patterns on the dune slope and dune top. The model results showed that most sediment would be deposited at the dune toe, and a (much) lesser amount would be deposited just landward of the dune crest. Moreover, little to no sediment transport and sedimentation was shown further landward (on top of the dune). This is in line with the results found from the Hondsbossche Dunes project.

## 6.2 Recommendations

As a final remark, the following recommendations for practical applications and further research are proposed:

- When sedimentation at the dune toe is desired in an artificial dune design, where initially no vegetation is present near the dune toe, the following advice is proposed from the results: a slope inclination of 20° and a dune toe orientation of 0° towards the dominant wind direction gives the most sedimentation around the dune toe, based on the results of this research. When more transport from the beach into the dune system is desired, the smallest incident wind angles and least steep slopes are optimal. However, with small incident wind angles, it is very important to have vegetation or another stabilization mechanism on the dune slope, especially near the dune crest, since speed-up over the dune slope causes strong erosion there.

- A more elaborate sensitivity analysis for roughness length and domain height could be done, to gain more complete knowledge on the influence of these parameters on the sediment transport patterns.

- Using the RNG $k$–$\epsilon$ turbulence closure model large differences are shown in bed shear stresses, especially on the dune top. This would influence the sedimentation occurring there significantly. Comparison with field or wind tunnel experiments could be done to test which model represents the shear stresses in the best way.

- An investigation into the impact of different dune shapes could be carried out. For example, attempts could be made to simulate different flow patterns seen in the field over differently shaped dunes using a CFD model. A possible first test case could be the flow pattern found by Davidson et al. (2022), who showed flow separation halfway on the dune slope by a change in slope. Moreover, scarps often have quite sharp edges at the crest. The effect of the sharpness of this top edge can be explored further.

- A short exhibition of the impact of vegetation on the sedimentation/erosion over the dune profile was shown in this research. More research could be done on how the introduction of vegetation and also moisture content change the results found in this research. This would likely lead to results that are better applicable for vegetated slopes.

- A coupling of this research with AeoLiS could be made, where the bed shear stress values from OpenFOAM are used to calculate more realistic sediment transport values and morphological changes with AeoLiS. A next step could be to create a morphological loop between the two programs, to take into account the morphological feedback to the flow and sediment transport patterns.

# References


Araújo, A. D., Parteli, E. J. R., Pöschel, T., Andrade, J. S., & Herrmann, H. J. (2013). Numerical modeling of the wind flow over a transverse dune. *Scientific reports*, *3*(1), 1–9.

Bagnold, R. A. (1937). The transport of sand by wind. *The Geographical Journal*, *89*(5), 409–438.

Bagnold, R. A. (1973). The nature of saltation and of 'bed-load' transport in water. *Proceedings of the Royal Society of London. Series A, Mathematical and Physical Sciences*, *332*(1591), 473–504.

Blocken, B., Stathopoulos, T., & Carmeliet, J. (2007). CFD simulation of the atmospheric boundary layer: Wall function problems. *Atmospheric Environment*, *41*, 238–252.

Bodde, W., Huiskes, R., IJff, S., Kramer, H., Kuiters, L., Lagendijk, G., Leenders, J., Ouwerkerk, S., Scholl, M., Smit, M., Smits, N., Stuurman, R., vd Valk, B., Verheijen, A., de Vries, D., & Wegman, C. (2019). Innovatieproject Hondsbossche Duinen: Eindrapportage. *ECOSHAPE / Wageningen Marine Research Rapport*, (C002/19).

Bodde, W., Leenders, J., Verheijen, A., & Wegman, C. (2018). B2-P2 - Analyse effecten maatregelen.

Cohn, N., Hoonhout, B. M., Goldstein, E. B., De Vries, S., Moore, L. J., Durán Vinent, O., & Ruggiero, P. (2019). Exploring marine and aeolian controls on coastal foredune growth using a coupled numerical model. *Journal of Marine Science and Engineering*, *7*(1), 13.

Davidson, S. G., Hesp, P. A., DaSilva, M., & Da Silva, G. M. (2022). Flow dynamics over a high, steep, erosional coastal dune slope. *Geomorphology*, *402*, 108111.

De Vries, S., Van Thiel de Vries, J. S. M., Van Rijn, L. C., Arens, S. M., & Ranasinghe, R. W. M. R. J. B. (2014). Aeolian sediment transport in supply limited situations. *Aeolian Research*, *12*, 75–85.

De Winter, W., Donker, J., Sterk, G., Beem, J., & Ruessink, G. (2020). Regional versus local wind speed and direction at a narrow beach with a high and steep foredune. *PLOS ONE*, *15*, e0226983.

Dong, Z., Liu, X., Wang, H., & Wang, X. (2003). Aeolian sand transport: A wind tunnel model. *Sedimentary Geology*, *161*(1-2), 71–83.

Durán, O., Claudin, P., & Andreotti, B. (2011). On aeolian transport: Grain-scale interactions, dynamical mechanisms and scaling laws. *Aeolian Research*, *3*(3), 243–270.

Durán, O., & Moore, L. J. (2013). Vegetation controls on the maximum size of coastal dunes. *Proceedings of the National Academy of Sciences*, *110*(43), 17217–17222.

Engineers Edge LLC. (2000). *Air density and specific weight table, equations and calculator* [Accessed: 15-08-2022]. https://www.engineersedge.com/calculators/air-density.htm

Hesp, P. A., & Smyth, T. A. (2016). Jet flow over foredunes. *Earth Surface Processes and Landforms*, *41*(12), 1727–1735.

Hesp, P. A., & Smyth, T. A. (2021). CFD flow dynamics over model scarps and slopes. *Physical Geography*, *42*(1), 1–24.

Hesp, P. A., Smyth, T. A., Nielsen, P., Walker, I. J., Bauer, B. O., & Davidson-Arnott, R. (2015). Flow deflection over a foredune. *Geomorphology*, *230*, 64–74.

Ho, T. D., Valance, A., Dupont, P., & El Moctar, A. O. (2011). Scaling laws in aeolian sand transport. *Physical Review Letters*, *106*(9), 094501.

Hoonhout, B. M., & Vries, S. d. (2016). A process-based model for aeolian sediment transport and spatiotemporal varying sediment availability. *Journal of Geophysical Research: Earth Surface*, *121*(8), 1555–1575.

Horikawa, K., Watanabe, A., & Katori, S. (1982). Sediment transport under sheet flow condition. *Coastal engineering 1982* (pp. 1335–1352).

Iversen, J. D., & Rasmussen, K. R. (1994). The effect of surface slope on saltation threshold. *Sedimentology*, *41*(4), 721–728.

Jackson, D., Cruz-Avero, N., Smyth, T., & Hernández-Calvento, L. (2013). 3D airflow modelling and dune migration patterns in an arid coastal dune field. *Journal of Coastal Research*, (65 (10065)), 1301–1306.

Jackson, P., & Hunt, J. (1975). Turbulent wind flow over a low hill. *Quarterly Journal of the Royal Meteorological Society*, *101*(430), 929–955.

Kawamura, R. (1951). Study on sand movement by wind. *The reports of the Institute of Science and Technology*, *5*, 95–112.

Kok, J. F., Parteli, E. J. R., Michaels, T. I., & Karam, D. B. (2012). The physics of wind-blown sand and dust. *Reports on progress in Physics*, *75*(10), 106901.

Largeau, J., & Moriniere, V. (2007). Wall pressure fluctuations and topology in separated flows over a forward-facing step. *Experiments in Fluids*, *42*(1), 21–40.

Lettau, K., & Lettau, H. (1978). Experimental and micrometeorological field studies of dune migration. *Exploring in the World's driest climate*, 110–147.

Nickling, W. G., & Neuman, C. M. (2009). Aeolian sediment transport. *Geomorphology of desert environments* (pp. 517–555). Springer.

Parsons, D. R., Walker, I. J., & Wiggs, G. F. S. (2004). Numerical modelling of flow structures over idealized transverse aeolian dunes of varying geometry. *Geomorphology*, *59*(1-4), 149–164.

Patankar, S. V., & Spalding, D. B. (1983). A calculation procedure for heat, mass and momentum transfer in three-dimensional parabolic flows. *Numerical prediction of flow, heat transfer, turbulence and combustion* (pp. 54–73). Elsevier.

Poppema, D. W., Wijnberg, K. M., Mulder, J. P., & Hulscher, S. J. (2018). Deposition patterns around buildings at the beach: Effects of building spacing and orientation. *Geomorphology*, *401*.

Pourteimouri, P., Campmans, G. H. P., Wijnberg, K. M., & Hulscher, S. J. M. H. (2022). A numerical study on the impact of building dimensions on airflow patterns and bed morphology around buildings at the beach. *Journal of Marine Science and Engineering*, *10*(1), 13.

Qian, G., Dong, Z., Luo, W., & Lu, J. (2011). Mean airflow patterns upwind of topographic obstacles and their implications for the formation of echo dunes: A wind tunnel simulation of the effects of windward slope. *Journal of Geophysical Research (Earth Surface)*, *116*, 4026–.

Qian, G., Dong, Z., Luo, W., Zhang, Z., & Zhao, A. (2012). Airflow patterns upwind of obstacles and their significance for echo dune formation: A field measurement of the effects of the windward slope angle. *Science China Earth Sciences*, *55*(4), 545–553.

Richards, P. J., & Hoxey, R. P. (1993). Appropriate boundary conditions for computational wind engineering models using the $k-\epsilon$ turbulence model. *Journal of wind engineering and industrial aerodynamics*, *46*, 145–153.

Roelvink, D., & Costas, S. (2019). Coupling nearshore and aeolian processes: XBeach and Duna process-based models. *Environmental Modelling & Software*, *115*, 98–112.

Sherman, D. J., Jackson, D. W. T., Namikas, S. L., & Wang, J. (1998). Wind-blown sand on beaches: An evaluation of models. *Geomorphology*, *22*(2), 113–133.

Sherman, D. J., & Li, B. (2012). Predicting aeolian sand transport rates: A reevaluation of models. *Aeolian Research*, *3*(4), 371–378.

Smith, A. B., Jackson, D. W. T., & Cooper, J. A. G. (2017a). Three-dimensional airflow and sediment transport patterns over barchan dunes. *Geomorphology*, *278*, 28–42.

Smith, A. B., Jackson, D. W. T., Cooper, J. A. G., & Hernández-Calvento, L. (2017b). Quantifying the role of urbanization on airflow perturbations and dunefield evolution. *Earth's Future*, *5*(5), 520–539.

Smyth, T. A. (2016). A review of computational fluid dynamics (CFD) airflow modelling over aeolian landforms. *Aeolian research*, *22*, 153–164.

Smyth, T. A., & Hesp, P. A. (2015). Aeolian dynamics of beach scraped ridge and dyke structures. *Coastal Engineering*, *99*, 38–45.

Strypsteen, G., Van Rijn, L. C., & Rauwoens, P. (2019). On the relation between predicted and observed aeolian transport rates: A field study at the belgian coast. *Aeolian Res*.

Troen, I., & Petersen, E. L. (1989). *European wind atlas*. Risø National Laboratory.

Tsoar, H. (1983). Wind tunnel modeling of echo and climbing dunes. *Developments in sedimentology* (pp. 247–259). Elsevier.

Tsoar, H., White, B., & Berman, E. (1996). The effect of slopes on sand transport — Numerical modelling. *Landscape and Urban Planning*, *34*(3-4), 171–181.

Van Bergen, J., Nijhuis, S., Mulder, J., & Wijnberg, K. (2020). Urban dunes: Promoting BwN dune formation at nourished beaches through spatial design. *Coastal Engineering Proceedings*, (36v), 23–23.

Van Rijn, L. C., & Strypsteen, G. (2020). A fully predictive model for aeolian sand transport. *Coastal Engineering*, *156*, 103600.

Walker, I. J., Davidson-Arnott, R. G. D., Hesp, P. A., Bauer, B. O., & Ollerhead, J. (2009a). Mean flow and turbulence responses in airflow over foredunes: New insights from recent research. *Journal of Coastal Research*, (SPEC. ISSUE 56), 366–370.

Walker, I. J. (2020). Aeolian (windblown) sand transport over beaches. In D. W. T. Jackson & A. D. Short (Eds.), *Sandy beach morphodynamics* (pp. 213–253). Elsevier.

Walker, I. J., Hesp, P. A., Davidson-Arnott, R. G. D., Bauer, B. O., Namikas, S. L., & Ollerhead, J. (2009b). Responses of three-dimensional flow to variations in the angle of incident wind and profile form of dunes: Greenwich Dunes, Prince Edward Island, Canada. *Geomorphology*, *105*(1-2), 127–138.

Walker, I. J., & Nickling, W. G. (2003). Simulation and measurement of surface shear stress over isolated and closely spaced transverse dunes in a wind tunnel. *Earth Surface Processes and Landforms: The Journal of the British Geomorphological Research Group*, *28*(10), 1111–1124.

# Appendices

# A Variation in wind speed and dune shape

In this chapter, the impact of variations in wind speed and dune shape are discussed.

## A.1 Variation in wind speed

The setup of the model described in section 3.1 ($U_{\text{ref}} = 20$ m/s and a dune height of 10 m) results in a flow with a Reynolds number in the order of $10^7$. This means the flow is in the fully turbulent domain. Consequently, even with low reference velocities of 5 m/s or more extreme reference velocities of 30 m/s, there will only be small changes in flow patterns over the dune. Thus, only changes in flow velocity magnitude are expected, but not in flow patterns such as speed-up factors and flow direction.
Simulations were done for a reference wind speed of 10, 15 and 20 m/s. In the sections below, the results are shown for wind flow patterns and bed shear stresses.

### A.1.1 Flow patterns

The speed-up factors ($|\vec{U}|/U_{\text{ref}}$) for the incident wind angles of 15° and 75° and a dune slope of 30° are shown in Figure A.1A. The lines almost completely cover each other, showing no relevant changes in speed-up over the dune between the different reference wind speeds. Moreover, the wind direction shown in Figure A.1B shows no changes over all incident wind angles between the different reference wind speeds. These results are equal for all dune slopes. In conclusion, the flow patterns do not change with a change in reference wind speed. Consequently, flow velocity results for a change in reference wind speed do not need a new simulation, since the flow velocities scale linearly with the reference wind speed. Moreover, wind direction results stay the same for different reference wind speeds.

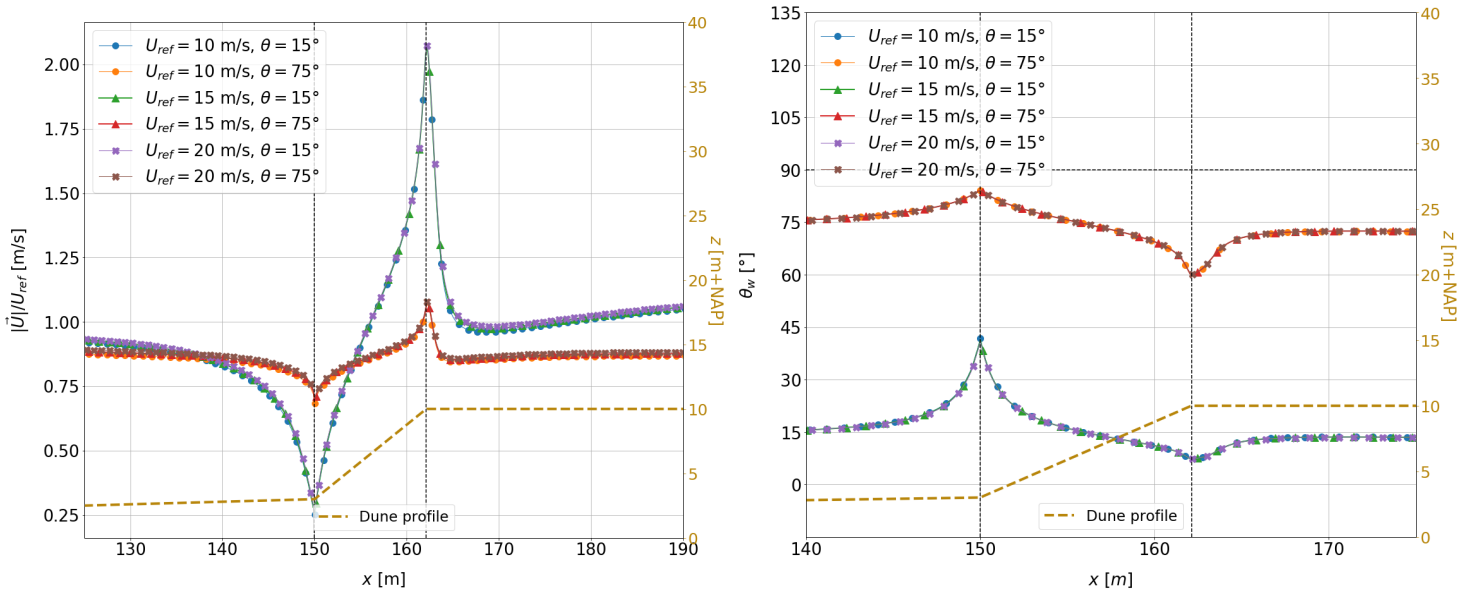


(A) (B)

FIGURE A.1: Flow patterns for a dune slope of 30° and varying wind directions for different reference wind speeds. (A) Speed-up over the dune profile ($|\vec{U}|/U_{\text{ref}}$, 25 cm above the surface). (B) Wind direction over the dune profile ($\theta_w$, 25 cm above the surface).

### A.1.2 Bed shear stresses

The other value that is desired from the OpenFOAM simulations is the bed shear stress ($\vec{\tau}$). Of course, it would be helpful if these values could also be calculated for other wind speeds without having to do more simulations. One of the ways to calculate the magnitude of the bed shear stress is to use the following equation:

$$|\vec{\tau}| = \rho u_*^2, \tag{12}$$

where $\rho$ is the fluid density and $u_*$ is the shear velocity. A standard way of relating the flow velocity at height $z$ ($U(z)$) to the shear velocity, is through the logarithmic wall function:

$$U(z) = \frac{u_*}{\kappa} \ln \frac{z}{z_0}, \tag{13}$$

where $\kappa$ denotes the von Kármán constant (0.41) and $z_0$ denotes the roughness height, or the height at which the velocity equals 0. This shows a linear relationship between $u_*$ and $U(z)$. Therefore, it is expected to see a quadratic relationship of the bed shear stress with the reference wind speed.

To show the differences between different reference wind speeds, the bed shear stress, normalized by a factor $U_{\text{ref}}^2$, for the incident wind angles of 15° and 75° and a dune slope of 30° are shown in Figure A.2A. The lines do not completely align, showing that the relationship is not purely quadratic. However, normalizing the bed shear stresses with a factor $U_{\text{ref}}^{1.9}$, shows much less differences between the different reference wind speeds. This is shown in Figure A.2B. Only on the dune top, a few meters landward of the dune crest, there are still some small discrepancies. These results are again equal for all dune slopes. In conclusion, the bed shear stress patterns do not change with a change in reference wind speed. Consequently, bed shear stress results for a change in reference wind speed do not need a new simulation, since the bed shear stress scales very well with a factor of $U_{\text{ref}}^{1.9}$, according to the aforementioned results.

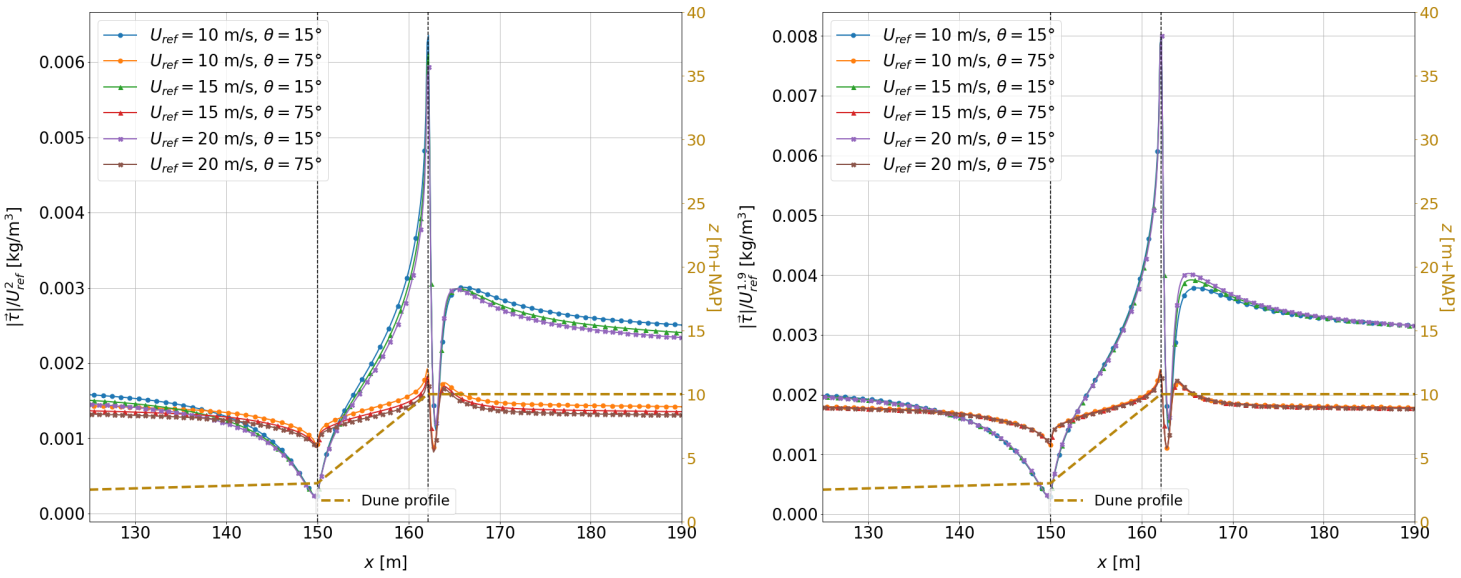


(A) (B)

FIGURE A.2: Normalized bed shear stress ($|\vec{\tau}|$) for a dune slope of 30° and varying wind directions for different reference wind speeds. The lines with the largest changes in shear stress indicate a 15° incident wind angle. The lines with the smallest changes indicate a 75° incident wind angle. The other lines show a 45° incident wind angle. (A) Bed shear stress normalized with $U_{\text{ref}}^2$. (B) Bed shear stress normalized with $U_{\text{ref}}^{1.9}$.

## A.2 Variation in dune shape

Simulations with two different dune shapes have been done: one with straight lines and sharp edges, and one with smoothed edges. An example of the grid with sharp edges, where the dune slope is equal to 40°, is shown in Figure A.3. The other grid setup is shown in Figure 10.

In this section, the results are shown for both shapes and the differences are highlighted. Figure A.4 shows the comparison between the two different setups in terms of cross-shore flow velocity for a dune slope of 40° and an incident wind angle of 0°. From the range of flow velocity of the sharp-edged setup (Figure A.4A), it follows that there is a negative flow velocity at the top of the dune. This can be explained by the fact that sharp edges induce flow separation much easier than smooth edges. Consequently, the flow has a reversal zone on top of the dune.

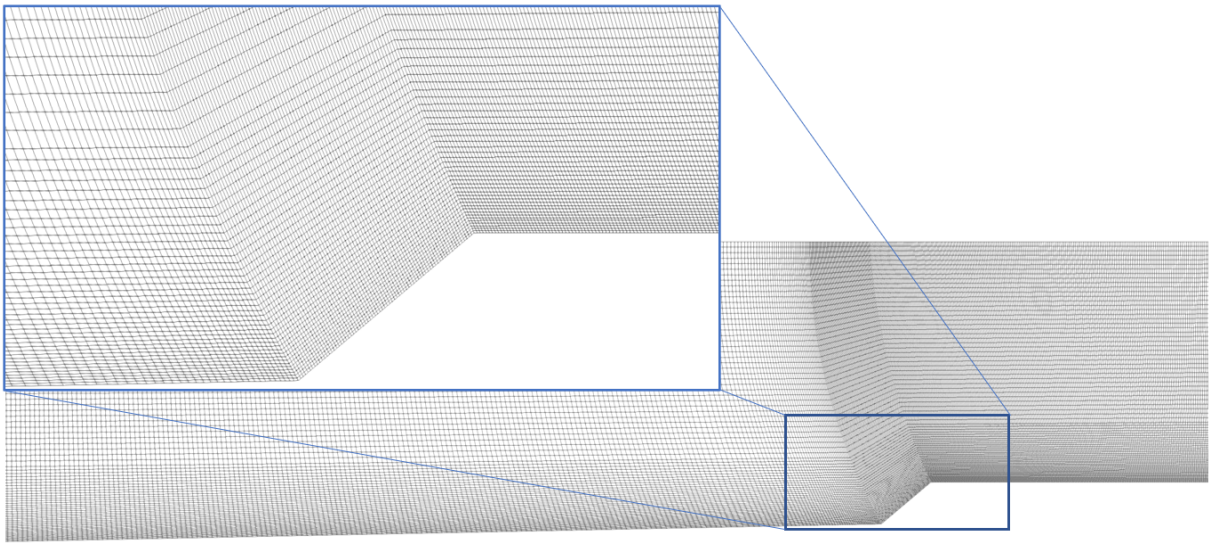

FIGURE A.3: Computational grid for the sharp-edged dune shape ($\gamma = 40°$). The highlighted box shows a close-up around the dune slope.

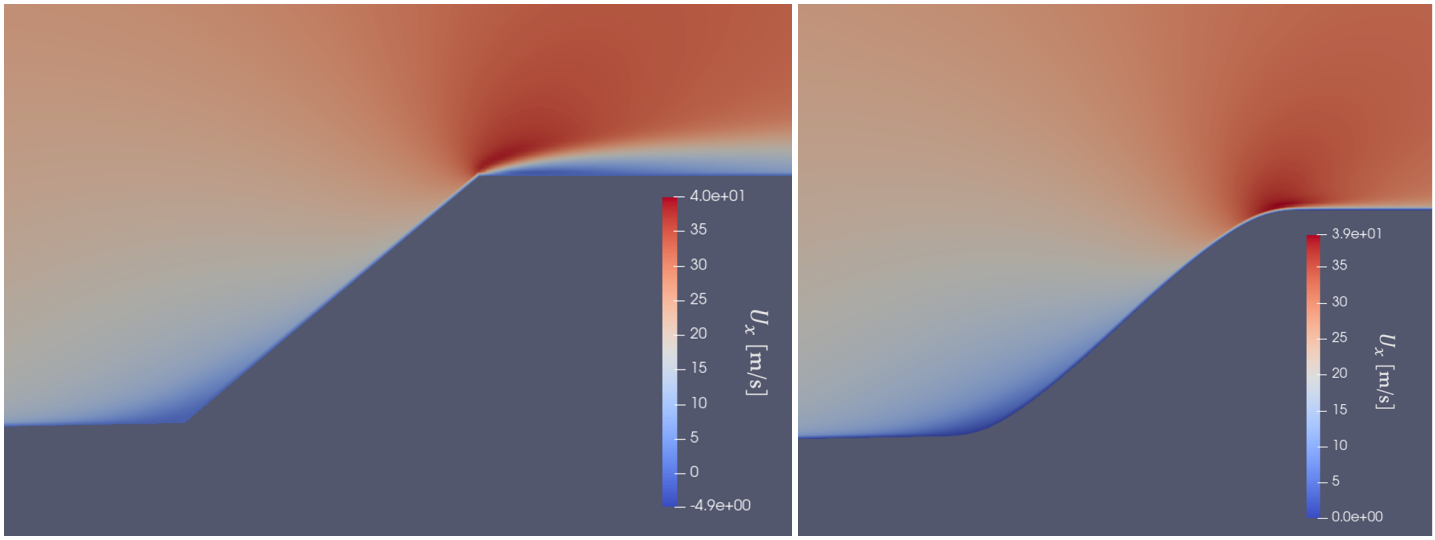


(A) (B)

FIGURE A.4: Cross-shore flow velocity ($U_x$) for a dune slope of 40° and an incident wind angle of 0°. (A) Sharp-edged dune setup. (B) Smooth-edged dune setup.

This result is seen for all dune slopes higher than 30° with a sharp-edged dune shape. However, for the smooth-edged dune shapes, the flow reversal at the dune top only occurs with much steeper dune slopes, at 70° and higher. Moreover, flow reversal at the dune toe for the sharp-edged setup occurs at a slope angle of 50° and higher, whereas in the smooth-edged case, it only occurs at a slope angle of 60° and higher. The difference in flow patterns over the dune for an angle of 50° is shown in Figure A.5. In conclusion, these results show how large the influence of the dune shape is to the flow patterns and therefore also to the sediment transport over the dune.

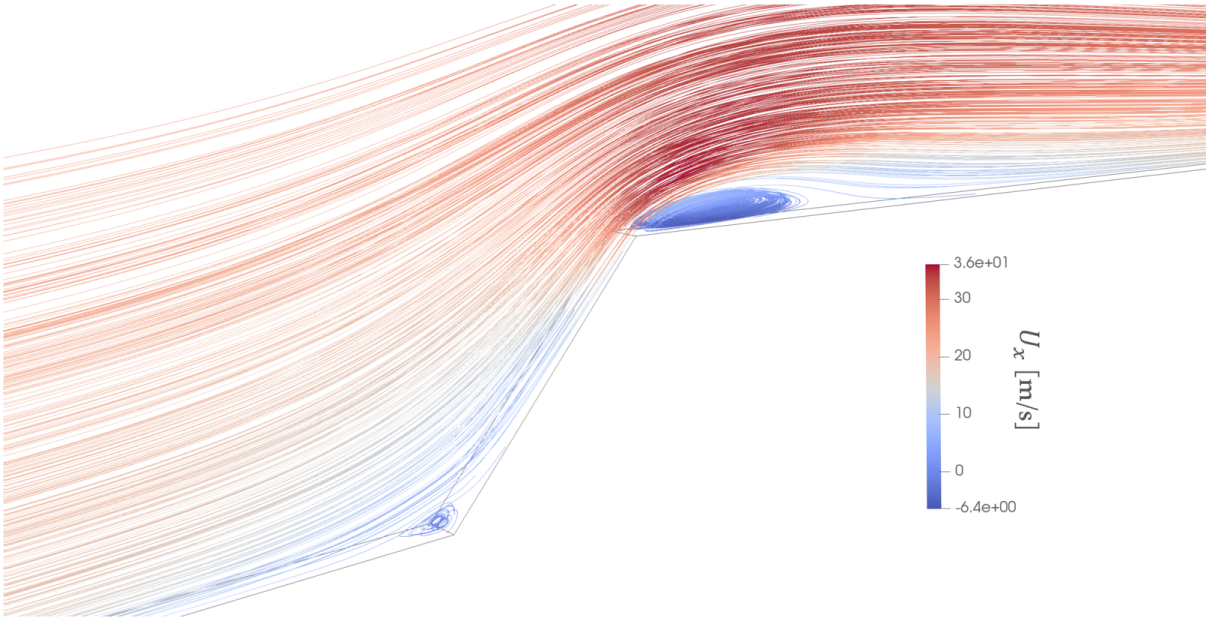


(A)

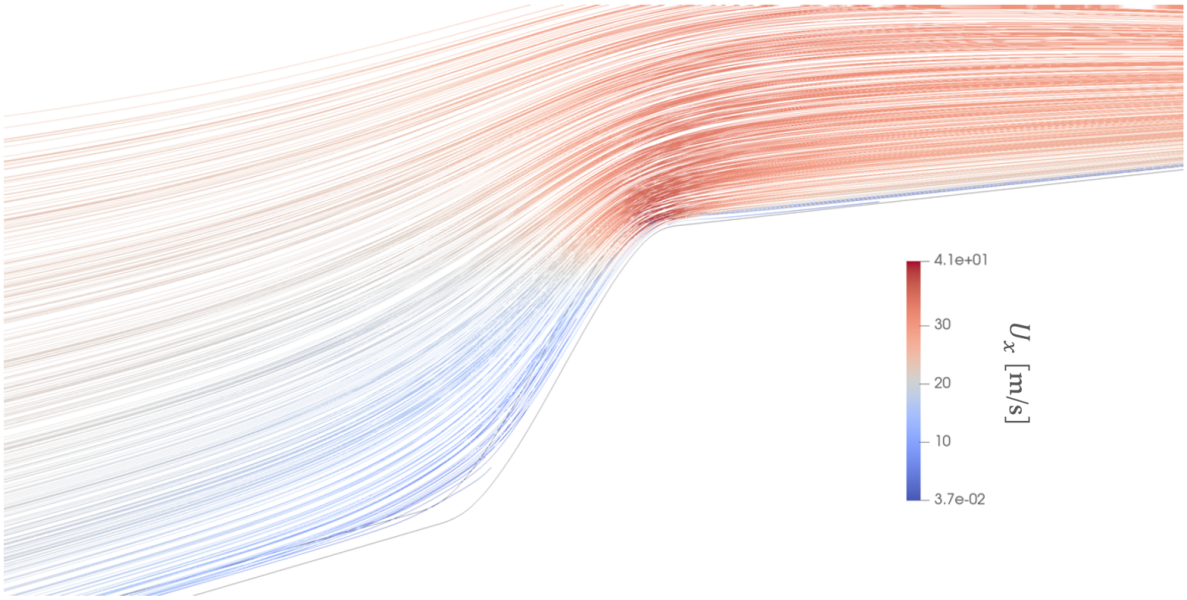


(B)

FIGURE A.5: Streamlines color-coded with cross-shore flow velocity for a dune slope of 50° and an incident wind angle of 0°. (A) Sharp-edged dune setup. (B) Smooth-edged dune setup.

# B Variation in grid setup

## B.1 Grid cell size

Test simulations were performed to produce a computational grid with the highest accuracy and the fastest convergence. Since the area in front of the dune is large and no quick changes in flow velocity or direction are present, the cells have a grading from the inlet towards the dune toe as to not have an unnecessary amount of grid cells. Also in the vertical direction, no quick changes in flow velocity or direction are present above approximately 10 m above the surface. Therefore, larger grid cells are applied higher up in the domain, and a grading is used towards the surface. Furthermore, because the flow is longshore uniform, a uniform grid cell size in that direction is chosen. See also Figures A.3 and 10 for a visual reference.
To ensure the results of each simulation were independent of mesh size, a comparison was done between different mesh sizes. Because there is grading involved in cross-shore and vertical directions, a range will be given for the mesh sizes in those directions. Only one of the comparisons will be shown here. The differences in respectively cross-shore, vertical and longshore wind speed are shown in Figure B.1. These plots show the flow velocity at 0.25 m above the surface. The grid cell dimensions in cross-shore, vertical and longshore direction for the coarser and the finer grid are shown in Table B.1. Especially in cross-shore and longshore direction, the change in velocity is substantial, but also only around the dune slope and on the dune crest. Subsequently, this substantiates the reasoning for the use of larger grid cells on the beach area. Further decreasing the mesh size only leads to very small changes. In conclusion, it was decided to use grid cell dimensions of (approximately) 0.15x0.1x0.1 m in the area on and around the dune slope, which contains the largest changes in flow velocity and direction.

## B.2 Domain depth

A check on the influence of domain depth (longshore beach length) was performed to see whether that has any influence on the simulation results. Three simulations were run, for a depth of 1 m, 2 m and 10 m, keeping the same cell size. These simulations show no large differences, as can be seen in Figure B.2. Therefore, a logical choice would be to use the shortest depth, because it results in less grid cells and therefore less computational time per simulation. In conclusion, it was decided to use a domain depth of 1 m (Figure 8).

TABLE B.1: Grid cell dimensions in meters over the domain for a coarser and finer grid. Arrows indicate a range in cell dimension from either left to right (→) or bottom to top (↑).

| | Region | Cross-shore | Vertical | Longshore |
|---|---|---|---|---|
| Original | Beach | 1.5 → 0.3 | 0.2 ↑ 0.75 | 0.2 |
| | Dune slope | 0.25 | 0.2 ↑ 0.75 | " |
| | Dune crest | 0.3 → 0.6 | 0.2 ↑ 0.6 | " |
| Refined | Beach | 0.8 → 0.2 | 0.1 ↑ 0.5 | 0.1 |
| | Dune slope | 0.15 | 0.1 ↑ 0.5 | " |
| | Dune crest | 0.15 → 0.3 | 0.1 ↑ 0.4 | " |

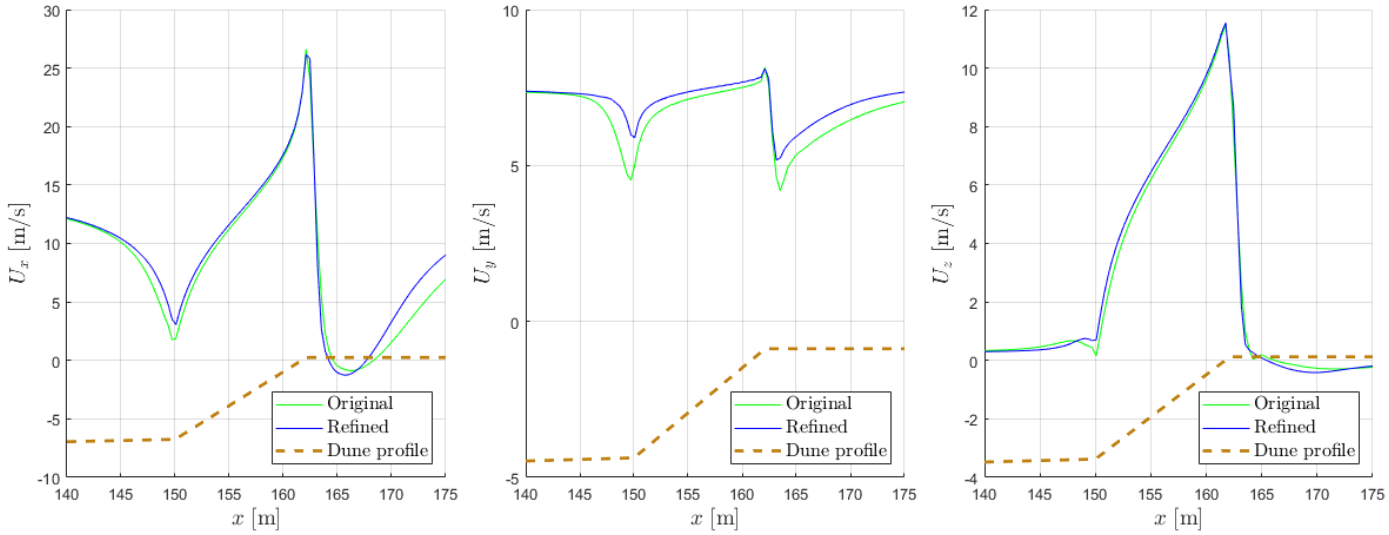


FIGURE B.1: Flow velocity in all directions ($U_x$, $U_y$, $U_z$, 25 cm above the surface) over the domain for the coarser ('Original') and the finer ('Refined') grid, as defined by Table B.1. From left to right: velocity in cross-shore, longshore and vertical direction, respectively.

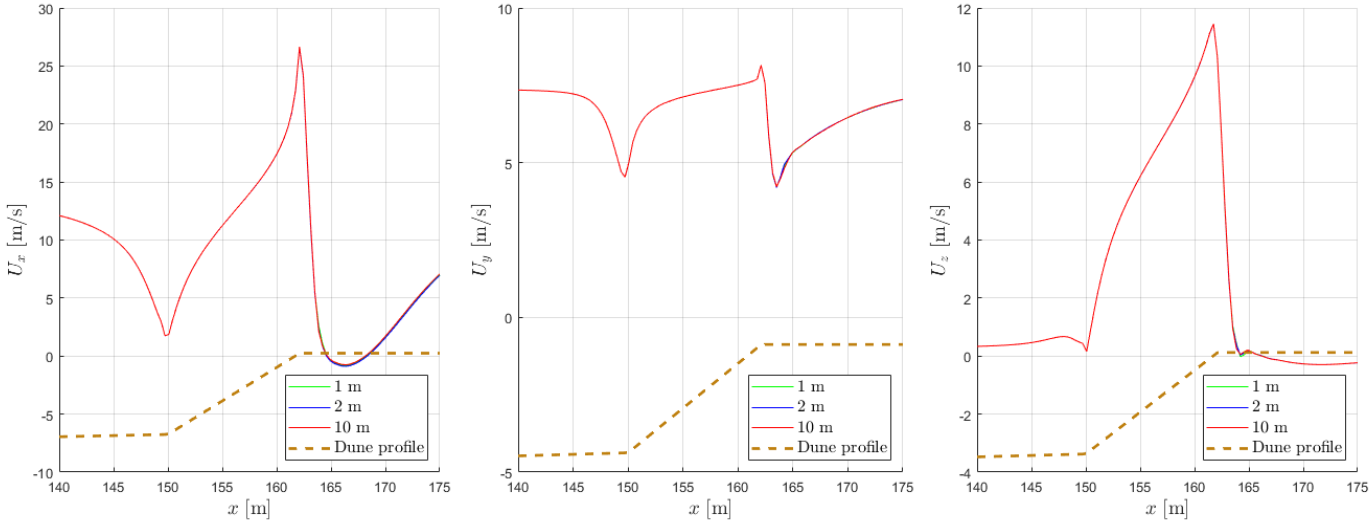


FIGURE B.2: Flow velocity in all directions ($U_x$, $U_y$, $U_z$, 25 cm above the surface) over the domain for a domain depth of 1 m, 2 m and 10 m. From left to right: velocity in cross-shore, longshore and vertical direction, respectively.

# C Numerical simulation settings

For the reproducibility of the simulation results, the most relevant numerical settings for the different parameters and the setup of the computational grid will be shown here.

## C.1 Parameter settings

The most relevant numerical parameter settings, which are gathered in the OpenFOAM `fvSolution` dictionary, are shown in Table C.1.

Different relaxation factors, which control under-relaxation, were tested to check the influence on the convergence of the simulation. Naturally, if the simulation converges, changes in the relaxation factor do not change the solution. However, it can lead to large changes in stability and therefore how fast and if the simulation converges to a solution. After different iterations and reading about multiple OpenFOAM simulations online, the relaxation factors were chosen, leading to stability and relatively fast convergence. The other parameters mentioned will be not be further explained here and are assumed to be known to people working with OpenFOAM.

Using these settings, the simulations finished on average in 10 minutes, with an average of 1500 iterations. The model runs were done on the computational cluster of Witteveen+Bos, using 16 cores with a clock speed of 2.84 GHz. This shows that an efficient use of the numerical possibilities of OpenFOAM and a good computer can lead to quite fast simulations, even with half a million grid cells. Therefore, it is possible for other researchers to quickly do multiple simulations to see the influence of a change of a specific parameter.

Another parameter that is used in the simulations is the kinematic viscosity ($\nu$), which was set to a value of $\nu = 1.48 \cdot 10^{-5}$ m$^2$/s.

TABLE C.1: OpenFOAM `fvSolution` settings for $U$, $k$, $\epsilon$ and $p$.

| *Parameter* | *Relaxation factor* | *Tolerance* | *Relative tolerance* | *Solver* | *Smoother* | *Residual control* |
|---|---|---|---|---|---|---|
| U | 0.95 | 1e-08 | 0.01 | `smoothSolver` | `symGaussSeidel` | 1e-5 |
| $k$ | 0.8 | 1e-06 | 0.01 | `smoothSolver` | `symGaussSeidel` | 1e-3 |
| $\epsilon$ | 0.8 | 1e-06 | 0.01 | `smoothSolver` | `symGaussSeidel` | 1e-4 |
| p | 0.5 | 1e-06 | 0.01 | `GAMG` | `GaussSeidel` | 1e-4 |

## C.2 Computational grid setup

Since the implementation of the dune in OpenFOAM is unique and not easily reproducible, the code of the `blockmesh` dictionary is added here.

```
/*--------------------------------*- C++ -*----------------------------------*\
| =========                 |                                                 |
| \\      /  F ield         | OpenFOAM: The Open Source CFD Toolbox           |
|  \\    /   O peration     | Version: v1812                                  |
|   \\  /    A nd           | Web:     www.OpenFOAM.com                       |
|    \\/     M anipulation  |                                                 |
\*---------------------------------------------------------------------------*/
FoamFile
{
    version     2.0;
    format      ascii;
    class       dictionary;
    object      blockMeshDict;
}

scale 1;
pi 3.14159;
```

```
beachL 150;
dunetoe 3;
crestL 50;
duneh 10;
ymax 50;
depth 1;
gamma ...;                // dune slope inclination in degrees
duneangle #calc "$gamma*$pi/180";
beachLtop #calc "$beachL-($ymax-$dunetoe)/tan(($pi-$duneangle)/1.85)";
dummy #calc "2*(tan($duneangle/2))/5 + 3*(tan($duneangle))/5";
duneL #calc "($duneh-$dunetoe)/($dummy)";
beachduneL #calc "$beachL + $duneL";
beachduneLtop #calc "$beachduneL-($ymax-$duneh)/tan(($pi-$duneangle)/1.85)";
xmax #calc "$beachduneL + $crestL";
interp1x #calc "($beachL+$beachLtop)/2";
interp1y #calc "$ymax/3";
interp2x #calc "($beachduneL+$beachduneLtop)/2";
interp2y #calc "($ymax-$duneh)/3+$duneh";

deltax 1;
deltay 1;
deltaz 0.1;

xcells2 #calc "round($duneL/cos($duneangle)/0.15)";
xcells3 #calc "round(220+15/cos($duneangle))";
zcells #calc "round($depth/$deltaz)";

vertices
(
    (0 0 0)                        // Vertex 0
    (0 $ymax 0)                    // Vertex 1
    ($beachL $dunetoe 0)           // Vertex 2
    ($beachLtop $ymax 0)           // Vertex 3
    ($beachduneL $duneh 0)         // Vertex 4
    ($beachduneLtop $ymax 0)       // Vertex 5
    ($xmax $duneh 0)               // Vertex 6
    ($xmax $ymax 0)                // Vertex 7
    (0 0 $depth)                   // Vertex 8
    (0 $ymax $depth)               // Vertex 9
    ($beachL $dunetoe $depth)      // Vertex 10
    ($beachLtop $ymax $depth)      // Vertex 11
    ($beachduneL $duneh $depth)    // Vertex 12
    ($beachduneLtop $ymax $depth)  // Vertex 13
    ($xmax $duneh $depth)          // Vertex 14
    ($xmax $ymax $depth)           // Vertex 15
);

posX
(
   (5 3 1)
   (1 1 0.2)
);
posY
(
   (1 1 4)
   (3 1 1)
);

blocks
(
    hex (0 2 3 1 8 10 11 9) (200 80 $zcells) simpleGrading ($posX $posY 1)
    hex (2 4 5 3 10 12 13 11) ($xcells2 80 $zcells) simpleGrading (1 $posY 1)
    hex (4 6 7 5 12 14 15 13) ($xcells3 80 $zcells) simpleGrading (2 $posY 1)
);

edges
(
     arc 2 3 ($interp1x $interp1y 0)
     arc 10 11 ($interp1x $interp1y $depth)
     arc 4 5 ($interp2x $interp2y 0)
     arc 12 13 ($interp2x $interp2y $depth)

   polyLine 2 4            // implement points on the curved slope
```

```
    (
     ...
    )

  polyLine 10 12          // implement points on the curved slope
    (
     ...
    )
);

boundary
(
    inlet
    {
        type patch;
        faces
        (
            (0 1 9 8) // Left
        );
    }
    outlet
    {
        type patch;
        faces
        (
            (7 6 14 15) // Right
        );
    }
    top
    {
        type patch;
        faces
        (
            (5 7 15 13) // Top
             (1 3 11 9)
             (3 5 13 11)
        );
    }
    bottom
    {
        type wall;
        faces
        (
            (2 0 8 10) // Bottom
             (2 10 12 4)
             (4 12 14 6)
        );
    }
    back
    {
        type cyclic;
        neighbourPatch front;
        faces
        (
            (8 9 11 10) // Back
             (10 11 13 12)
             (12 13 15 14)
        );
    }
    front
    {
        type cyclic;
        neighbourPatch back;
        faces
        (
            (1 0 2 3) // Front
             (3 2 4 5)
             (5 4 6 7)
        );
    }
);
```